



1 **Bayesian age-depth modelling applied to varve and radiometric**
2 **dating to optimize the transfer of an existing high-resolution**
3 **chronology to a new composite sediment profile from Holzmaar**
4 **(West-Eifel Volcanic Field, Germany)**

5 Stella Birlo^{1*}, Wojciech Tylmann², Bernd Zolitschka¹

6 1 - University of Bremen, Institute of Geography, GEOPOLAR, Bremen, Germany

7 2 - University of Gdańsk, Faculty of Oceanography and Geography, Gdańsk, Poland

8 *Corresponding author: sbirlo@uni-bremen.de



9 Abstract

10 This study gives an overview of different varve integration methods with Bacon. These techniques
11 will become important for the future as technologies evolve with more sites being revisited for
12 the application of new and high-resolution scanning methods. Thus, the transfer of existing
13 chronologies will become necessary, because the recounting of varves will be too time consuming
14 and expensive to be funded.

15 We introduce new sediment cores from Holzmaar (West-Eifel Volcanic Field, Germany), a volcanic
16 maar lake with a well-studied varved record. Four different age-depth models (A-D) have been
17 calculated for the new composite sediment profile (HZM19) using Bayesian statistics with Bacon.
18 All models incorporate new Pb-210 and Cs-137 dates for the top of the record, the latest
19 calibration curve (IntCal20) for radiocarbon ages as well as the new age estimation for the Laacher
20 See Tephra. Model A is based on previously published radiocarbon measurements only, while
21 Models B-D integrate the previously published varve chronology (VT-99) with different
22 approaches. Model B rests upon radiocarbon data, while parameter settings are obtained from
23 sedimentation rates derived from VT-99. Model C is based on radiocarbon dates and on VT-99 as
24 several normal-distributed tie-points, while Model D is segmented into four sections: Sections 1
25 and 3 are based on VT-99 only, whereas Sections 2 and 4 rely on Bacon age-depth models
26 including additional information from VT-99. In terms of accuracy, the parameter-based
27 integration Model B shows little improvement over the non-integrated approach, whereas the tie
28 point-based integration Model C reflects the complex accumulation history of Holzmaar much
29 better. Only the segmented and parameter-based age-integration approach of Model D adapts and
30 improves VT-99 by replacing sections of higher counting errors with Bayesian modelling of
31 radiocarbon ages and thus efficiently makes available the best possible and precise age-depth
32 model for HZM19. This approach will value all ongoing and high-resolution investigations for a
33 better understanding of decadal-scale Holocene environmental and climatic variations.

34 Keywords: Lacustrine sediments, Varves, Bayesian age-depth modelling, Bacon, Radiometric
35 dating



36 **1. Introduction**

37 Terrestrial archives from lakes have the potential to provide information about climate and the
38 human history of its catchment area beyond instrumental and historical data. In the late 1980s,
39 piston coring and freeze coring techniques for lacustrine sediment records have improved
40 tremendously allowing a better quality of sediments to be recovered from modern lakes. Since
41 then, the new fields of limnogeology and paleolimnology flourished with increasing demand of
42 societies for documentation of natural background data related to questions around acid rain,
43 environmental pollution and more and more with a focus on global climate change.

44 To provide such information not only on local scales but also on larger regional to global scales,
45 investigations from different sites need to be compared and linked. However, such correlations
46 are only successful if the contributing archives are based on robust chronologies. Therefore,
47 precise and reliable age-depth models are the basis for sedimentary investigations and
48 reconstructions of environmental and climatic changes of the past, as they ensure intra-site
49 comparability and enable recognition of larger scale patterns. A reliable chronology should be
50 based on a combination of different dating techniques (multiple dating approach) such as
51 radiometric dating, well-known event layers (e.g., tephrochronology), historic data (e.g., flood
52 events) or varve counting. The term “varve” (Swedish: layer) was first introduced by De Geer
53 (1912) for outcrops with proglacial sediments and describes finely laminated sediment structures
54 with annual origin. The alternating pale and dark layers are driven by seasonal changes in
55 temperature and precipitation that cause different chemical and biological processes within the
56 lake and its catchment area. When anoxic conditions at the sediment-water-interface are given at
57 least seasonally, i.e. no bioturbation destroys laminations, varves are preserved and provide high-
58 resolution and precise chronologies in calendar years (Zolitschka et al., 2015).

59 Until the 1980s, varve chronologies were the only option for calendar-year chronologies for
60 sediment records, while AMS radiocarbon dating was still in its infancy and calibration of
61 radiocarbon ages was restricted to the Middle and Late Holocene, if at all applied. First reviews
62 about methodological advances in the study of annually laminated sediments appeared at the
63 same time (Anderson and Dean, 1988; O’Sullivan, 1983; Saarnisto, 1986) and long varve-dated
64 reconstructions were published for Elk Lake, USA (Dean et al., 1984) and Lake Valkiajärvi, Finland
65 (Saarnisto, 1985). Meerfelder Maar and Holzmaar were the first varve-dated lacustrine records
66 covering the entire Holocene and the Late Glacial for Central Europe (Zolitschka, 1989, 1988),
67 followed by records concentrating on the Late Glacial to Holocene transition at Soppensee,
68 Switzerland (Lotter, 1991) and at Lake Gosciarz, Poland (Goslar et al., 1993). As such, the Holzmaar
69 record became one of the best studied lacustrine records in Europe, if not world-wide. Since the
70 first coring campaign in 1984, several sediment records have been recovered from Holzmaar and



71 numerous studies were carried out with sedimentological, biological, geochemical and
72 geophysical methods (e.g. Zolitschka, 1989; Lottermoser et al., 1993; Hajdas et al., 1995;
73 Raubitschek et al., 1999; Leroy et al., 2000). However, the early sediment records from Holzmaar,
74 although counted and corrected multiple times, still contain sections of high counting uncertainty
75 and thus suffer from optimal core correlation as it is possible today by applying high-resolution
76 scanning techniques and digital line-scan images. Moreover, independent time control of varve
77 chronologies with AMS radiocarbon dating became available only in the 1990s (Hajdas-
78 Skowronek, 1993), while Bayesian age-depth modelling established as a tool for optimizing dating
79 efforts only during the last decade (Ramsey, 2009) and sediment scanning revolutionized
80 limnogeology and paleolimnology over the last 20 years. Therefore, we revisited Holzmaar to
81 obtain fresh sediment cores for the conduction of innovative and high-resolution (sub-millimetre-
82 scale) sediment scanning techniques to be based on an improved age-depth model.

83 As chronologies are always a “running target”, especially as new scientific methods and
84 approaches appear, it is no wonder that the varve chronology for Holzmaar sediments has
85 developed from its first attempt as “Varve Time 1990” (VT-90) (Zolitschka, 1990) to VT-99 ten
86 years later (Zolitschka et al., 2000). In the course of applying ultra-high (sub-mm-scaled)
87 resolution scanning techniques to the new set of sediment cores from Holzmaar (HZM19), VT-99
88 was transferred to HZM19 making use of marker layers and radiocarbon ages for correlation as
89 well as of Bayesian age-depth modelling for the creation of an updated varve chronology (VT-22).

90 Different to earlier studies, we make use of available radiocarbon dates from Holzmaar not only
91 to correct the varve chronology but to combine it with the independent radiocarbon chronology
92 using Bayesian modelling. This integration approach is not commonly used for lacustrine records.
93 Here we select three different methods to integrate varve and radiometric dating and apply it to
94 the Holzmaar data. We concentrate on approaches using the Bacon package for the R statistical
95 programming software (Blaauw and Christen, 2011), whereas literature also provides
96 comparable methods for alternative Bayesian age-depth modelling software, such as OxCal
97 (Martin-Puertas et al., 2021; Ramsey, 2008; Vandergoes et al., 2018), which was also used to
98 integrate varve counting and radiometric dating for the Holocene sediment record HZM96-4a,4b
99 from Holzmaar (Prasad and Baier, 2014).

100 In this study we discuss the possibilities to integrate and improve different chronologies by
101 combining a varve chronology with modelling approaches. This is accomplished by testing and
102 comparing integration methods with regard to accuracy and precision from the interpolated varve
103 chronology itself and for a Bayesian model without any varve information. With this integration
104 of all age information we produce the most reliable age estimations for the HZM19 record: VT-22.
105 Based on the best model outcome, this master chronology serves as the chronological base for



106 ongoing and future biological, geochemical and geophysical investigations conducted on the new
107 Holzmaar sediment cores (e.g. García et al., 2022).

108 2. Materials and Methods

109 2.1 Regional Setting

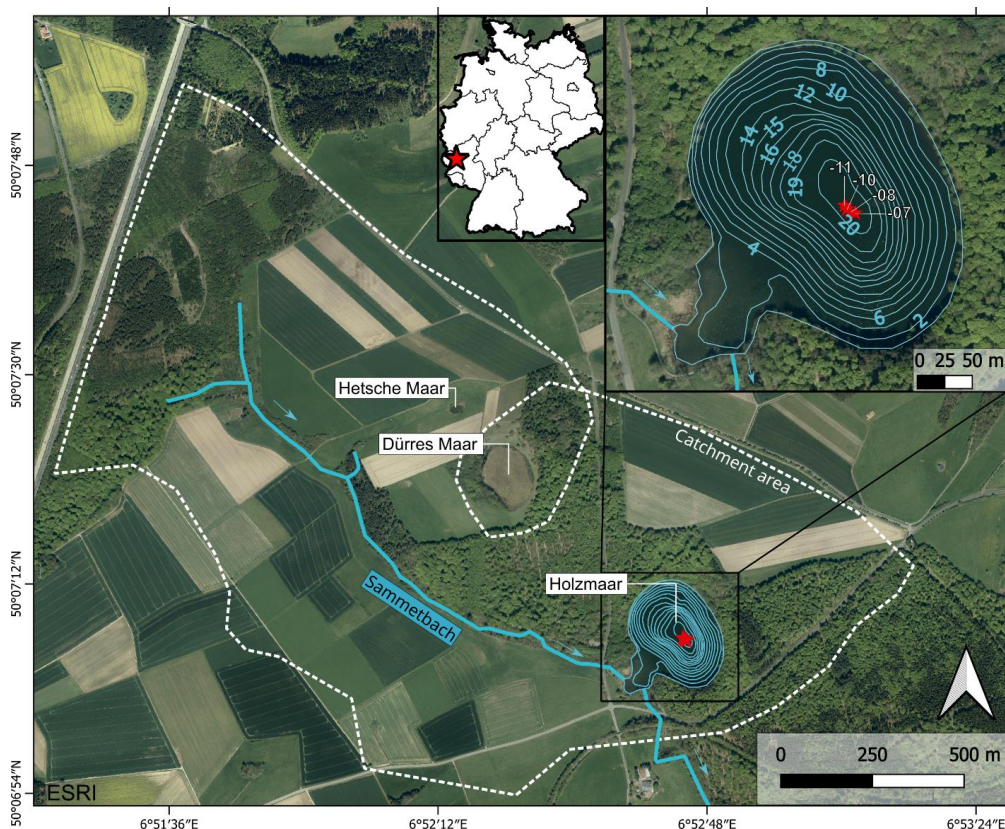
110 The late Quaternary volcanic maar lake Holzmaar (425 m a.s.l., 50°7'8" N, 6°52' 45" E) is located
111 in the western central part of the Rhenish Massif in the West-Eifel Volcanic Field (WEVF;
112 Rhineland-Palatinate, Germany, Fig. 1). The WEVF consists of more than hundred volcanic cones
113 and maars, of which only nine are water-filled today (Meyer, 2013; Schmincke, 2014). The
114 volcanism in the Eifel region was caused by uplift of the Rhenish Shield since 700 - 800 ka, which
115 started in the NW near Ormont (Meyer and Stets, 2002; Schmincke, 2007). Volcanic activities
116 reached a peak at ca 600 – 450 ka in the central WEVF and then decreased towards Bad Bertrich
117 in the SE (Schmincke, 2007). The uplift is responsible for many eruptive centres at NW-SE
118 trending tectonic faults, along which several phreatomagmatic maar explosions occurred (Büchel,
119 1993; Lorenz, 1984; Lorenz et al., 2020; Meyer, 1985). One of these eruptions formed the
120 Holzmaar system ca. 40 - 70 ka ago (Büchel, 1993) consisting of three maars with the maar lake
121 of Holzmaar, the raised bog of Dürres Maar and the dry Hetsche or Hitsche Maar (from SE to NW).
122 With 100 m in diameter, the latter is the smallest maar of the WEVF (Fig. 1).

123 The catchment area of Holzmaar (2.06 km²) includes the Sammetbach, a creek that flows in and
124 out of the lake. Due to the low erosive energy of the stream no delta formed in the lake (Scharf,
125 1987; Zolitschka, 1998a). The geology in the catchment area consists of Devonian metamorphic
126 slates, greywackes and quartzites as well as Quaternary loess and volcanic rocks related to
127 eruptions of the Holzmaar system (Meyer, 2013). Holzmaar is located within a conservation area
128 since 1975 protecting the surrounding beech forest (*Fagus sylvatica* L.), while ca. 60% of the
129 catchment area is in agricultural use (Kienel et al., 2005).

130 Holzmaar has a diameter of 300 m (water surface: 58,000 m²) and with a maximum water depth
131 of 19-20 m shows a deep and steep-sided morphology typical for maar lakes. Only a small and
132 shallow embayment in the SW interrupts the nearly circular and 1100 m long shoreline. This
133 appendix-like bay developed due to an artificial damming in the late Middle Ages, which was
134 constructed to supply a downstream water mill (Zolitschka, 1998a). For the last glacial,
135 paleolimnological investigations indicate oligotrophic conditions, but eutrophication started
136 already at the onset of the Late Glacial (García et al., 2022). During the Holocene, water quality is
137 affected by human activities, which started during the Neolithic (around 6500 cal. BP) according
138 to pollen analysis (Litt et al., 2009). Together with the inflow of the Sammetbach this caused a
139 steady but slow process of eutrophication and today leads to meso- to eutrophic conditions (Lücke



140 et al., 2003; Scharf and Oehms, 1992; Zolitschka, 1990). The lake is holo- and dimictic with an
141 anoxic hypolimnion during summer stratification (Scharf and Oehms, 1992). Altogether, this
142 caused a high potential for varves to be formed and preserved.



143
144 *Figure 1: ESRI Satellite image of the Holzmaar volcanic system and its catchment area (indicated by a white dashed line)*
145 *with Holzmaar, Dürres Maar, Hetsche Maar and Sammetbach (blue line, flow direction indicated by arrows). Upper left*
146 *insert: Location of Holzmaar in Germany (red star). Upper right insert: Bathymetric map with isobaths in meter and coring*
147 *locations (HZM19-07, -08, -10 and -11) marked by red stars.*

148 2.2 Sediment core collection

149 In August 2019 Holzmaar was revisited and four parallel cores (HZM19-07, HZM19-08, HZM19-
150 10, HZM19-11) have been retrieved from the centre of the lake in 19 m water depth (Fig. 1) using
151 a UWITEC piston-corer with a diameter of 90 mm (HZM19-07, -08, -10) and 60 mm (HZM19-11)
152 from a coring platform. The water-sediment interface was perfectly recovered with HZM19-07-
153 01 as the piston stopped 15 cm above the sediment surface. At the GEOPOLAR lab (University of
154 Bremen) the cores have been split in halves lengthwise, photographed and visually described
155 using a Munsell colour chart and according to the description guide line by Schnurrenberger et al.



156 (2003). Cross correlation of all sediment-core sections was conducted macroscopically using
157 distinct layers.

158 2.3 Chronology

159 2.3.1 Evolution of the Holzmaar varve chronology

160 First varve counts and documentation of the annual origin for the finely laminated sediments
161 preserved in the Holzmaar record were carried out in the late 1980's (Zolitschka, 1990, 1991,
162 1992), presenting the initial Holocene and Late Glacial varve chronology VT-90. Varve Time (VT)
163 refers to varve (calendar) years before 1950 CE (Common Era), which is equivalent to the
164 commonly used reference timescale for radiocarbon dates provided in cal. BP (calibrated years
165 before present, i.e. 1950 CE). The chronology of VT-90 was elaborated for the HZM84-B/C
166 composite record recovered in 1984 and was counted back to the onset of the Late Glacial, i.e. to
167 12,794 VT-90. This varve chronology was subsequently extended by counting the deeper,
168 periglacial section back to the Last Glacial Maximum, i.e. to an age of 22,500 VT-90 (Brauer, 1994;
169 Brauer et al., 1994).

170 By including the new sediment cores of HZM90-E/-F/-H, VT-90 was modified resulting in VT-94.
171 These overlapping sediment-core series as well as all other mentioned cores have been recovered
172 from the deepest part of Holzmaar, i.e. from within the 20-m isobath (Fig. 1). This recounting
173 revealed an underestimation of the youngest 5000 years, for which 555 years have been added.
174 This initial underestimation was mainly caused by sections with very thin varves difficult to count
175 (Zolitschka, 1998b). Another discrepancy occurred within the sediments of the Younger Dryas
176 (YD), for which 245 years had to be added. Altogether, the difference from VT-90 to VT-94
177 comprises an addition of 800 years, shifting the basal age of the Late Glacial back to 13,594 VT-94
178 (Zolitschka, 1998b).

179 To crosscheck the varve chronology with an independent dating method, 41 samples of terrestrial
180 macrofossils along the entire profile (Tab. A2) have been analysed using the AMS (Accelerator
181 Mass Spectroscopy) radiocarbon method (Hajdas et al., 1995 and one unpublished radiocarbon
182 date). A comparison between VT-94 and the calibrated radiocarbon chronology shows a
183 discrepancy of +346 years between 3500 and 4500 VT-94 (Hajdas et al., 1995; Hajdas-Skowronek,
184 1993). This correction factor was estimated by Chi²-minimization and added by linear
185 interpolation between 3500 and 4500 VT-94. The outcome was VT-95, which consists of three
186 segments. Segment I is covered by an "absolute" chronology until 3500 VT-95, while segment II
187 (3500 - 4846 VT-95) was extended based on the discrepancy detected between varve and
188 calibrated radiocarbon chronologies. Segment III covers sediments from 4846 - 13,940 VT-95 and
189 is considered as a floating chronology (Hajdas et al., 1995; Zolitschka, 1998b).



190 In 1996 new sediment cores (HZM96-4a, -4b) have been obtained from Holzmaar and VT-95 was
191 transferred to this new record using 26 distinct marker layers with their related VT and error. The
192 age-depth model was subsequently obtained by linear interpolation (Baier et al., 2004). At the
193 same time, novel varve counts for the Meerfelder Maar sediment record established 1880 varve
194 years between the two isochrones of Laacher See Tephra (LST, eruption ca 40 km NE from
195 Holzmaar) and Ulmener Maar Tephra (UMT, eruption ca 13 km NE from Holzmaar) (Brauer et al.,
196 1999), which both are also archived in the Holzmaar sediment record. However, this well-
197 constrained time interval was only 1560 years long for the Holzmaar record. The obviously
198 missing 320 years have been positioned and added to VT-95 based on pollen data from Holzmaar
199 (Leroy et al., 2000), assuming a hiatus for the middle part of the YD biozone at 12,025 VT-95. This
200 results in the latest version (VT-99) of the Holzmaar varve chronology (Zolitschka et al., 2000)
201 with a basal age of 14,260 VT-99 for the Late Glacial.

202 Varve quality and error estimations were first discussed and described based on multiple counts
203 of selected and representative thin sections (Zolitschka, 1991). Later, different varve quality
204 classes have been described in more detail for VT-90 (Zolitschka et al., 1992) and for VT-95
205 (Zolitschka, 1998b) with error estimations in the 1σ range (Table A1). Similar error margins were
206 confirmed by counting more recent sediment profiles (HZM96-4a, 4b) from Holzmaar (Prasad and
207 Baier, 2014). In this study, the uppermost part was discussed as showing even higher counting
208 uncertainties. However, no alternative error margins were provided for this section. Thus, we use
209 the data of Table A1 for further evaluations.

210 **2.3.2 Transfer of VT-99 to HZM19**

211 The varve chronology VT-99 (Zolitschka et al., 2000) was transferred to HZM19 by using 43
212 predefined marker layers and 41 radiocarbon sampling positions analysed by Hajdas et al. (1995,
213 2000) with their specific VT-99 ages and errors (Tables A1, A2). Both, marker layers and
214 radiocarbon sampling positions have been identified and justified by comparison with documents
215 describing the samples as well as core photographs from previous studies and sediment profiles,
216 such as HZM90-E, -F, -H and HZM96-4a, 4b. All marker layers cover an age range from 141 to
217 14,158 VT-99. After assignment, the ages of the marker layers have been linearly interpolated and
218 cumulative counting errors were calculated based on the 1σ errors provided with Table A1.

219 **2.3.3 Pb-210 and Cs-137 dating**

220 The isotopes Pb-210 and Cs-137 have been used to radiometrically date the uppermost part of
221 HZM19 at the University of Gdansk. In total, 61 samples were taken with a thickness of 2 cm. The
222 activity of Cs-137 was determined directly by gamma-ray spectrometry from freeze-dried and
223 homogenized samples. Gamma measurements were carried out using a HPGe well-type detector
224 (GCW 2021) with a relative efficiency of 27% and full width at half maximum (FWHM) of 1.9 at



225 the energy of 1333 keV (Canberra). Energy and efficiency calibration were done using reference
226 material CBSS-2 (Eurostandard CZ) in the same measurement geometry like the samples. The
227 counting time for each sediment sample was 24 hours.
228 Activity of total Pb-210 was determined indirectly by measuring Po-210 using alpha
229 spectrometry. Dry and homogenized sediment samples of 0.2 g were spiked with a Po-209 yield
230 tracer and digested with concentrated HNO₃, HClO₄ and HF at a temperature of 100 °C using a CEM
231 Mars 6 microwave digestion system. The solution obtained was evaporated with 6M HCl to
232 dryness and then dissolved in 0.5M HCl. Polonium isotopes were spontaneously deposited within
233 four hours on silver discs. Activities were measured using a 7200-04 APEX Alpha Analyst
234 integrated alpha-spectroscopy system (Canberra) equipped with PIPS A450-18AM detectors.
235 Samples were counted for 24 hours. A certified mixed alpha source (U-234, U-238, Pu-239 and
236 Am-241; SRS 73833-121, Analytics, Atlanta, USA) was used to check the detector counting
237 efficiencies.

238 **2.3.4 Bayesian age-depth modelling**

239 To produce the chronology for HZM19 we test and compare different methods integrating varve
240 counts with radiometric measurements using Bayesian age-depth modelling. The advantage of
241 any modelling approach is that all possible calendar ages of calibrated radiocarbon dates and their
242 probability density functions (PDFs) will be tested by using a repeated random sampling method
243 (Blaauw, 2010; Telford et al., 2004). In addition, using the Bayes theorem allows to incorporate
244 information of the accumulation history known prior to modelling. Thus, calendar ages, which are
245 monotonic with depth and with positive accumulation rates in yr cm⁻¹ (in sedimentological terms,
246 accumulation rates as they are used for Bayesian age-depth modelling are equivalent to
247 "sedimentation rates", as corroborated by the units used) are calculated (Lacourse and Gajewski,
248 2020; Trachsel and Telford, 2017). This is different if compared to the "Classical Age-depth
249 Modelling" carried out by CLAM (Blaauw, 2010).

250 Currently established programs that use Bayesian statistics are Oxcal (Ramsey, 2008), BChron
251 (Haslett and Parnell, 2008) and Bacon (Blaauw and Christen, 2011), all of which differ in terms of
252 parameter settings and handling of outliers. In this study, we focus on varve counting integration
253 methods using Bacon (rBacon version 2.5.7; Blaauw et al., 2021; Blaauw and Christen, 2011) for
254 the R programming language (version 4.1.1; R Core Team, 2021). Bacon uses a Markov Chain
255 Monte Carlo (MCMC) sampling strategy to model the accumulation history piecewise using a
256 gamma autoregressive semi-parametric model (Blaauw and Christen, 2011). The accumulation
257 rate of each segment depends on the accumulation rate of the previous segment. Dates are treated
258 using a student's t-distribution. Although Bacon provides default values, the accumulation rate is
259 controlled by two adjustable prior distributions (prior model), the accumulation rate as a gamma



260 distribution and the memory, which describes the dependence of accumulation rates between
261 neighbouring depths as a beta distribution. Both latter parameters are defined by a shape and a
262 strength prior, respectively, in addition to a mean prior. Furthermore, we make use of the number
263 of segments (thick-parameter) recommended by Bacon. The program also allows to incorporate
264 information about hiatus and slump events in the profile.

265 Only few studies use the Bayesian approach that integrates varve counting information with
266 radiocarbon dates. We extracted three different methods and for comparison include one model
267 only with radiocarbon data, i.e. excluding any VT-99 information. Thus, four different age-depth
268 models (A-D) are compared and discussed:

269 A) Model based only on radiocarbon dates.

270 B) This parameter-based varve integration method introduced by Vandergoes et al. (2018)
271 compares several varve integration techniques for sediments from Lake Ohau (New Zealand)
272 using both OxCal and Bacon. Here, we select the integration approach with Bacon, where the
273 “varve counts function” is the source for the prior-parameter of mean accumulation rate. Major
274 changes in accumulation history recorded by the varve data are derived by using the R package
275 “segmented” (Muggeo, 2022). It dissects the sediment sequence and for each resulting segment
276 an individual mean accumulation-rate prior is defined.

277 C) The tie point-based integration used by Shanahan et al. (2012) integrates the varve chronology
278 from Lake Bosumtwi (Ghana) based on certain tie points with normally distributed age
279 uncertainties of the cumulative error. They address the problem of integrating all individual varve
280 counts, as they cannot be considered as independent chronological datapoints. Thus, they would
281 be weighted too strongly in the model. The compromise we have chosen for this study, is placing
282 one varve tie-point every 100 years. As there is no varve counting available for HZM19 but VT-99
283 ages based on marker layers, we implement them with cumulative errors as tie points instead.

284 D) The segmented and parameter-based integration introduced by Bonk et al. (2021) provides
285 the most complex method for varve integration. The problem of not or poorly varved sections in
286 the sediment profile of Lake Goszcz (Poland) is compensated by dividing the profile into three
287 sections and interpolating the section with low-quality varves using Bayesian modelling. For the
288 Holzmaar record, we define four sections: sections 2 and 4 are based on Bayesian modelling, while
289 sections 1 and 3 rely on VT-99. Section 3 is treated as a floating chronology and placed based on
290 the sum of calibrated radiocarbon probabilities lying within this section. To tighten the two
291 Bayesian modelled sections to the following varved sections, an anchor tie-point based on the
292 oldest age of the younger sections is implemented.



293 For each model we use the calibration curve IntCal20 (Reimer et al., 2020) and make use of the
294 default accumulation strength and memory priors. We also implement a surface age of -69 ± 1
295 cal. BP as tie point with a normal distributed error to anchor the chronology to present-day.

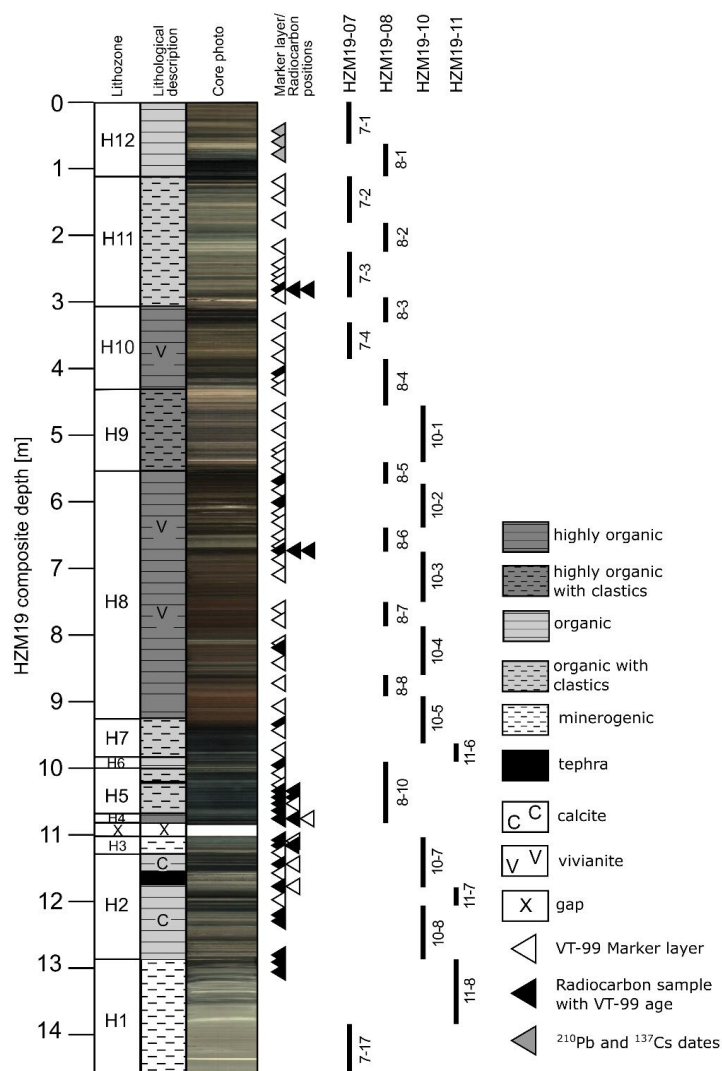
296 **3. Results and Interpretation**

297 **3.1 Lithology**

298 The four parallel cores HZM19-07, -08, -10 and -11 were aligned and correlated to form the
299 composite profile HZM19 (Fig. 2), which includes 24 core sections and reaches to a basal depth of
300 14.64 m (Table A3). One technical sediment gap exists at a composite depth of 10.90 m. To
301 determine the precise length of this gap, we use core photographs from a previous Holzmaar
302 core (HZM90-H5u) and determined the technical gap with a length of 12.9 cm (Fig. A1).

303 The lithological description of HZM19 follows the characterization of Zolitschka (1998a, 1998b),
304 dividing the HZM84-B/C profile into 12 lithozones (H1 – H12). Except H1, all lithozones cover
305 finely-laminated diatomaceous gyttja with varying minerogenic and organic content and colour.
306 All lithozone depths are summarized in Table A4. The transition from light greenish grey (10Y
307 8/1) and greyish brown (2.5Y 5/2) minerogenic, finely laminated, weakly carbonaceous silts and
308 clays in H1 (12.9 – 14.6 m) to carbonaceous laminated gyttja in light olive brown (2.5Y 5/3), black
309 (10YR 2/1) and light-yellow brown (2.5Y 6/3) with slightly higher organic content in H2 (11.3 –
310 12.9 m) indicates the transition from the Pleniglacial to the Late Glacial.

311 Within H2, the distinct and almost 20 cm thick coarse-grained tephra from the Laacher See
312 eruption (LST, 11.5 – 11.7 m) is deposited, a well-dated isochrone (Reinig et al., 2021) of European
313 lake sediments. The following lithozone H3 (10.9 – 11.3 m) shows a high minerogenic content
314 and almost no organic components with colours of light greenish grey (5GY 7/1) and grey brown
315 (10YR 5/2), representing the YD at the end of the Pleistocene. Unfortunately, almost one third
316 (12.9 cm) of the YD lithozone H3 is missing due to a technical gap.



317

318 *Figure 2: Composite profile of HZM19 with (from left to right) lithozones H1 to H12 (cf., Table A4), lithological description,*
 319 *core photographs taken immediately after core splitting, positions of marker layers and radiometric samples (cf., Tables*
 320 *A2, A5) and core sections used for the composite profile (cf., Table A3).*

321 The Holocene sediment shows a periodic change from sections with higher organic content in
 322 black (2.5Y 2.5/1) and light olive brown (2.5Y 5/3) (H4: 10.7 – 10.9 m, H6: 9.9 – 10.0 m) to sections
 323 with high organic and clastic content in slightly brighter colours like grey (10YR 5/1) (H5: 10.0 –
 324 10.7 m, H7: 9.3 – 9.9 m). The tephra of the Ulmener Maar eruption (UMT, ca. 3 mm thick) occurs
 325 in H5 at 10.24 m. The longest lithozone H8 (5.5 – 9.3 m) contains distinctly varved dark reddish
 326 brown (5YR 3/2) sediments with high organic content changing towards the top to very dark



327 greyish brown (10YR 3/2) and brown (10YR 4/3) with several up to 5 mm thick lenses of
328 authigenic vivianite. Also, a low carbonate content was recognized. Furthermore, turbidites are
329 observed more frequently from H8 to the top of HZM19.

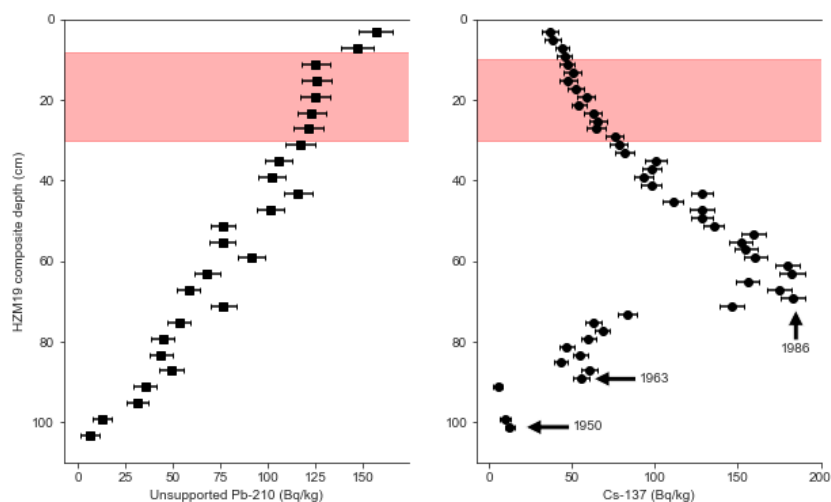
330 Above H8, the clastic content increases and brightens up to light olive brown (2.5 Y 5/3) and
331 greyish brown (2.5Y 5/2) hues in H9 (4.3 – 5.5 m). In H10 (3.1 – 4.3 m) colours change to darker
332 hues, e.g. olive grey (5Y 4/2) and black (5Y 2.5/2), while the organic content remains high and
333 terrestrial macrofossils like pieces of wood or leaf remains occur more frequently towards the
334 top. The organic content is decreasing slightly in H11 (1.1 – 3.1 m), which also contains clastic
335 components and terrestrial plant material as well as turbidites with paler colours, e.g. olive brown
336 (2.5Y 5/3) and grey (2.5Y 5/1). The uppermost lithozone H12 (1.1 m to the top of HZM19) shows
337 unconsolidated organic sediment with a homogenous blackish (5Y 2.5/1) colour for the lower
338 part and brighter dark olive grey (5Y 3/2) sediment at the very top.

339 **3.2 Chronology**

340 **3.2.1 Pb-210 and Cs-137 dating**

341 The profile of unsupported Pb-210 activity concentration shows a gradual rather than an
342 exponential decrease within the first meter of HZM19 (Fig. 3). Additionally, a plateau from 8 to
343 30 cm is interpreted as a section with rapid deposition of homogenous material and will be
344 treated for further analyses as a slump event. Despite this irregularity, the gradual decrease in
345 unsupported Pb-210 activity with depth indicates high sedimentation rates. We use the CFCS
346 (Constant Flux Constant Sedimentation) model to estimate mean sedimentation rates of
347 $1.09 \pm 0.13 \text{ cm yr}^{-1}$. This value should be treated with caution but suggests that the uppermost
348 meter (including a 22 cm-thick slump) was deposited in ca. 70 years.

349



350

351 *Figure 3: Results of unsupported Pb-210 (left) and Cs-137 (right) measurements with error bars for the uppermost 110 cm*
352 *of HZM19. Shaded areas indicate the plateau shown by Pb-210 data, black arrows mark peaks assigned to*
353 *radiochronological events (given numbers are ages in years CE).*

354 The variability of Cs-137 activity concentrations delivers potentially three historical markers
355 (Fig. 3). The Cs-137 profile is smooth lacking sharp peaks due to high sedimentation rates and
356 likely sediment focusing. First traces of Cs-137 are recognizable at 101.2 cm and indicate atomic
357 bomb testing in the early 1950's. At 89.2 cm, there is a significant increase signalling
358 atmospheric fallout in the early 1960's in response to peak atomic bomb testing. Finally, at 69.2
359 cm a strong increase in Cs-137 documents the 1986 Chernobyl accident (Fig. 3, Table A5). This
360 interpretation is generally in line with the results of Pb-210 dating. The shape of the Cs-137
361 record also corresponds nicely to the results of Sirocko et al. (2013), who measured Cs-137 on
362 sediments from Schalkenmehrener Maar and Ulmener Maar (both WEVF). For both of these
363 cases, the 1986 Chernobyl peak is also much larger than the one related to the start of atomic
364 bomb tests in 1963.
365

366 3.2.2 Varve time and independent radiocarbon chronology

367 The varve chronology VT-99 was transferred to HZM19 using 84 marker layers of which 41 are
368 radiocarbon dating positions. These marker layers distribute in HZM19 from 1.16 - 12.93 m and
369 cover the VT-99 age range from 141 to 14,158 VT-99 (Table A2). During the transfer of marker
370 layers to HZM19 and comparison between HZM19 and previous Holzmaar sediment cores
371 (HZM84-B/C, HZM92-E/-F/-H, HZM96-4a/4b) differences in position of the lowermost marker



372 layers occurred. All records show differences in distances between marker layers (ML) 1 (14,156
373 VT-99), ML-2 (14,152 VT-99) and ML-3 (13,646 VT-99) making a clear assignment of these layers
374 difficult. Thus, we excluded these three marker layers for the transfer of VT-99 to HZM19. The
375 lowermost applied marker layer is therefore ML-4 with a varve age of 13,087 VT-99 at a depth of
376 11.86 m. Because of inconsistencies in documentation, we excluded two more VT-99 ages, i.e.
377 those related to the radiocarbon ages HZM-46 and HZM-10.1 (Table A2).

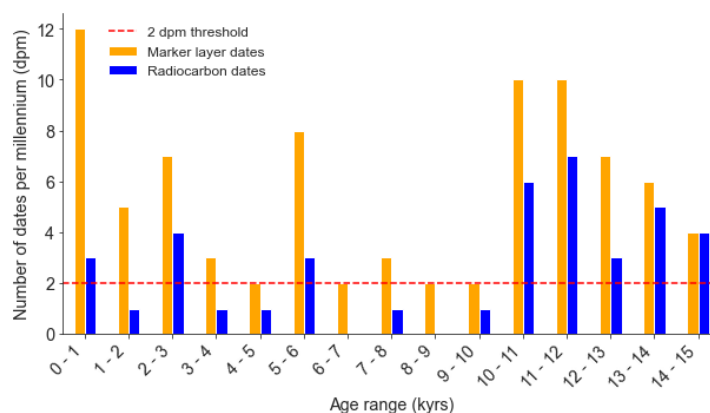
378 The marker layer density reaches a mean value of 5.5 dpm (dates per millennium) being most
379 frequent before 10,000 and after 6000 cal. BP (Fig. 4). We use a linear interpolation to receive an
380 age-depth model based only on VT-99 with a resulting accuracy of 282 years as a mean age range
381 and a maximum age range of 744 years (Table A6).

382 The radiocarbon dating density of HZM reaches an overall mean value of 2.7 dpm (Fig. 4), which
383 is 35% higher than the 2 dpm recommended for Bayesian modelling by Blaauw et al. (2018).
384 However, their distribution is uneven. Radiocarbon dates are most frequent for ages >10,000 cal.
385 BP with 3-7 dpm (mean: 5 dpm) (Fig. 4). A minimum density of radiocarbon dates (0-1 dpm) is
386 obtained from 10,000-6000 cal. BP (mean: 0.5 dpm). Therefore, a chronology based on the
387 available radiocarbon data within this section should be interpreted with caution. Dating density
388 for the uppermost 6000 years is higher and varies between 1 and 4 dpm (mean: 2.2 dpm).

389 When we compare VT-99 with radiocarbon ages calibrated with the latest calibration curve
390 IntCal20 (Reimer et al., 2020), an overall agreement with marker layers is observed. Only for the
391 lowermost part below approximately 10.64 m at radiocarbon sample HZM-46 (Table A2), we
392 observe an increasing underestimation of VT-99 in relation to IntCal20 calibrated radiocarbon
393 ages (Fig. A2, Table A2). This was already observed by Hajdas et al. (2000) in comparison to
394 Intcal98 but has not been corrected yet.



395



396

397 *Figure 4: Number of dating points per millennium (dpm) of HZM19 for marker layers (n: 84, mean: 5.5 dpm) and*
398 *radiocarbon dates (n: 41, mean: 2.7 dpm). Red dotted line marks the recommended threshold of 2 dpm for Bayesian*
399 *modelling suggested by Blaauw et al. (2018). Surface age and three ages estimated by Cs-137 are excluded.*

400 3.2.3 Age-depth modelling

401 Four different Bayesian age-depth models are calculated, of which three include varve ages
402 (Model B-D) and one only radiocarbon ages (Model A). In common for all model runs are the
403 default memory priors and the use of the IntCal20 calibration curve (Reimer et al., 2020).
404 Furthermore, based on the Pb-210 and Cs-137 dating analysis, a slump at a composite depth of 8-
405 30 cm was implemented, as well as the LST from 11.52 – 11.71 m. As known from previous varve
406 and pollen studies of the Holzmaar record (Brauer et al., 1999; Leroy et al., 2000), 320 years are
407 missing during the YD and have been included into VT-99 at 12,025 VT-99. Based on the study of
408 Leroy et al. (2000), we were able to locate the position of the YD hiatus to a depth of 11.09 m,
409 which we implemented for each model with a maximum duration of 320 years. In addition to
410 marker layers and radiocarbon dates, we included the surface age of -69 ± 1 cal. BP and three
411 events dated by Cs-137 (Table A5).

412 Preliminary test runs reveal two necessary changes to be made for the calculations: 1) The default
413 number of iterations is too low to produce a robust model for the entire HZM19 sediment
414 sequence. Thus, we use the *Baconvergence()*-function of Bacon to estimate the number of
415 iterations needed. This function repeats the calculations and tests if the MCMC mixing of the core
416 results in a robust model by calculating the “Gelman and Rubin Reduction Factor” (Brooks and
417 Gelman, 1998). Good mixing is indicated by a threshold of <1.05, which in our case was reached
418 after three iterations when the number of iterations was increased to 40,000. This results in a
419 better mix of MCMC iterations but also in long calculation times (> 5 hours). 2) For each test run,
420 Bacon predicted ages consistently too old for the LST, which is probably caused by slightly too old



421 ages of the surrounding radiocarbon dates (Table A2). To gain a better comparability with studies
422 from other sites, we decided to include the latest LST age of 13,006 \pm 9 cal. BP (Reinig et al., 2021,
423 Table A5).

424 In addition, we extended the age-depth model to a maximum depth of 14.64 m, as ongoing
425 analyses exceed the lowermost dated level. However, in the following chapters we only discuss
426 the model output between the first (ML36/1) and the last (HZM-19) marker layer at 12.93 m
427 (Table A2) and compare it with the interpolated varve chronology (VT-99).

428 After each calculation and if the Bacon output indicates a highly variable log of objectives or MCMC
429 iterations, we made use of the scissor() command to achieve a better mixing of the output. All
430 Bacon model outputs with their settings and additional information are shown in Fig. A3 and
431 related ages are listed in Table A6.

432 The **model without varve integration (Model A)** is based on the year of sediment recovery
433 (surface age), three dates estimated by Cs-137 analyses, the age for the LST (Reinig et al., 2021)
434 and 41 calibrated radiocarbon probability density functions (Fig. A3A). Different to Hajdas et al.
435 (1995), this model includes the outlier of HZM-23, but excludes HZM-24 and other described
436 outliers (Table A2).

437 Model A results in an age of 14,615 [minimum: 14,339, maximum: 14,926] cal. BP at the
438 lowermost dated depth of 12.93 m with a mean age uncertainty of 468 yrs. The maximum age
439 uncertainty of approx. 1056 years occurs at a depth of 8.86 m within lithozone H8 (Table A6),
440 where radiocarbon dating density is <1 dpm (Fig. 4).

441 The **parameter-based integration (Model B)** integrates VT-99 using all dates as in Model A and
442 adjusts the prior information given for the calculation based on the varve accumulation-history.
443 We follow the procedure presented by Vandergoes et al. (2018) and calculate a breakpoint based
444 on ages and depths of the marker layers at 4.43 m, i.e. at 1312 VT-99 (Fig. A3B). This boundary is
445 implemented as an additional hiatus to the Bacon code with a duration of 1 year. The accumulation
446 rate prior is set based on published sedimentation rates (Zolitschka et al., 2000). We calculate
447 with a mean of 0.49 yr/mm for the uppermost part (71-1312 VT-99), with 1.30 yr/mm from 1312
448 to the YD hiatus at 12,025 VT-99 and with 0.76 yr/mm from the YD hiatus to the lowermost age
449 of 14,158 VT-99. Model B is calculated using the same parameters as for Model A and with the
450 same treatment of outliers.

451 The resulting posterior model shows similarities to Model A, having a maximum mean age of
452 14,456 [min.: 14,236, max.: 14,749] cal. BP at a depth of 12.93 m and a mean 95% confidence
453 interval of 456 years with a maximum of 1064 years at 8.78 m, i.e. within the period of lowest
454 radiocarbon dating density (Fig. 4).



455 The **tie point-based integration (Model C)** is based on the approach used by Shanahan et al.
456 (2012). We include 43 marker layers with related VT-99 ages and cumulative errors as normal
457 distributed tie points into the model, which adds to the dates used in Models A and B and sums up
458 to 89 dates. This approach increases the amount of chronological information and fills areas with
459 larger gaps between radiocarbon dates. The model was run with default settings provided by
460 Bacon (Fig. A3C). Bacon recognizes the outliers in the same way as by previously described
461 models.

462 Model C results in a maximum age of 14,614 [min.: 14,332, max.: 14,919] cal. BP (at 12.93 m) with
463 a mean 95% confidence interval of 329 years, which is better than for Models A and B. A maximum
464 age range of 749 years is given at a depth of 9.18 m, which is also slightly better than for previously
465 presented models. However, Model C produced MCMC iterations with highest noise and it was
466 difficult to cut out a well-mixed section (Fig. A3C, upper left panel).

467 The **segmented and parameter-based integration (Model D)** is a more complex method of
468 varve integration used by Bonk et al. (2021) and was adapted for the HZM19 profile by dividing
469 the varve chronology of VT-99 into four sections. This separation is based on variations of
470 counting uncertainty, radiocarbon sampling density and an increasing offset of VT-99 to the latest
471 calibration curve IntCal20 (Fig. A2).

472 Section 1 (0 – 5.98 m) and Section 3 (6.70 – 9.90 m) are transferred and interpolated based on VT-
473 99 marker layers, as they are consistent with calibrated radiocarbon data (Section 1) and have
474 well-preserved varves with small counting errors of $\pm 0.7\%$ (Section 3). Section 2 (5.98 – 6.70 m)
475 and Section 4 (9.9 – 14.6 m) are reported as showing higher counting uncertainties (Section 2) or
476 increasing differences between VT-99 and the calibration curve (Section 4). Thus, we replace the
477 varve chronology in Sections 2 and 4 with Bayesian age-depth modelling (Fig. A3D). Section 4 also
478 contains very dense radiocarbon dates (Hajdas et al., 2000), which increase the predictability of
479 Bacon (Fig. 4).

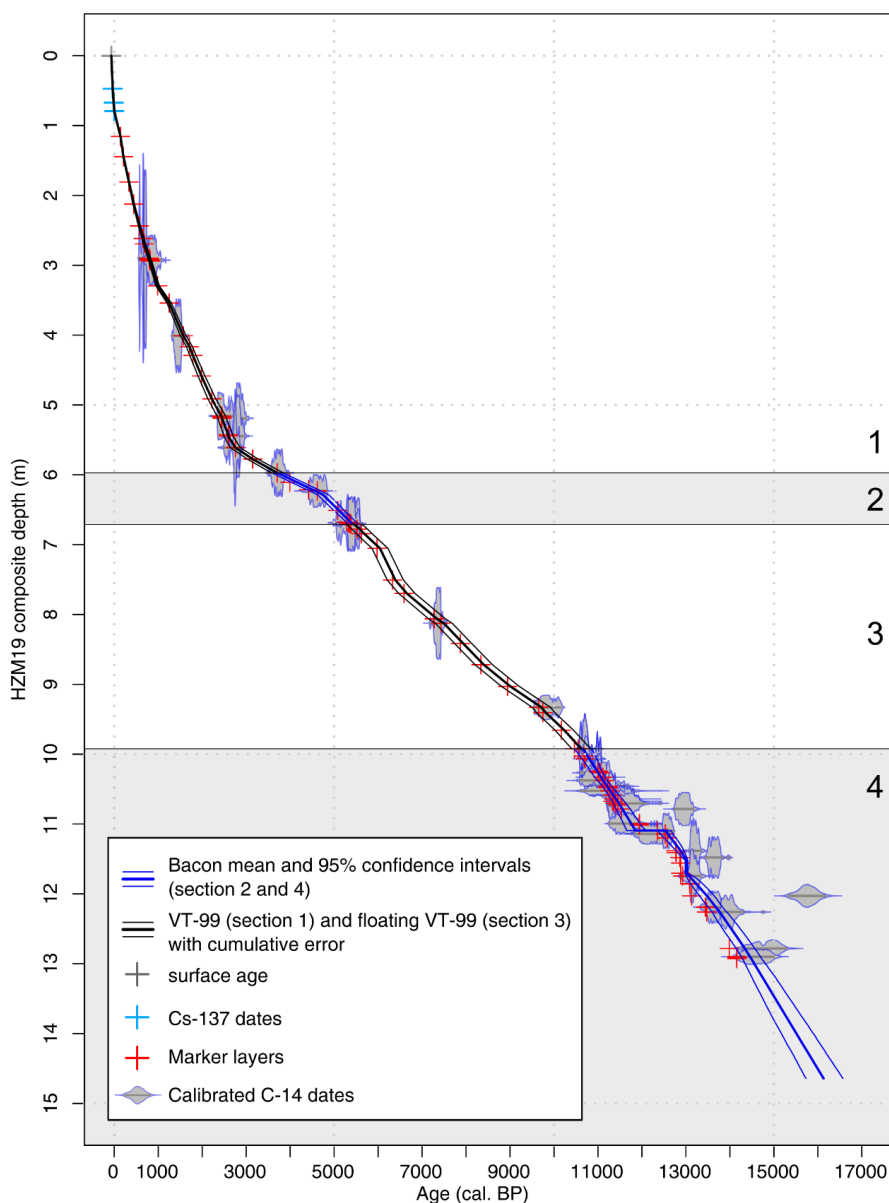
480 Section 1 is based on linear interpolation for ages of the sediment surface (-69 ± 1 cal. BP), three
481 dates derived by Cs-137 analyses (Table A5) and 25 ages of marker layers with a basal age of 3704
482 ± 134 cal. BP at the position of HZM-25 (Table A2).

483 The modelled Section 2, previously identified as a section with sedimentation rates >2.86 yr/mm
484 and therefore a source of high counting uncertainties and underestimation of varve ages
485 (Zolitschka et al., 2000), consists of five radiocarbon dates (Table A2) and the basal age of Section
486 1 (3704 ± 134 cal. BP) as anchor point for Section 2. To reduce the resulting gap between first and
487 second sections, we reduce the error estimation for the anchor point to ± 70 years ($+0.5\sigma$). As
488 there is a major change in sedimentation rates within this section, we calculated a boundary



489 similar as in Model B using the marker layers of this section (Fig. A3D). This allows defining a
490 boundary at the depth of 6.29 m with adjusted accumulation means of 3.33 yr/mm above (5.98 –
491 6.29 m) and 1.59 yr/mm below (6.29 – 6.70 m), using published sedimentation rate data
492 (Zolitschka et al., 2000). Based on suggestions by the software, the “thick”-parameter was set to 4
493 mm. The resulting model covers and age range from 3709 [min.: 3591, max.: 3825] to 5419 [min.:
494 5329, max.: 5548] cal. BP (Fig. A3D section 2).

495 Section 3 interpolates 16 marker layers (Table A2), which are treated as a floating chronology.
496 The placement of the anchor point relates to the basal age of the lowermost calibrated
497 radiocarbon date (HZM-4.3) in Section 2 (Table A2) and the maximum sum of the four calibrated
498 radiocarbon PDFs within this part with a summed probability of 0.076 at 5450 ± 165 cal. BP (Fig.
499 A4 A).



500

501 *Figure 5: Age-depth model for HZM19 based on Model D with Sections 1 and 3 based on VT-99 (section numbers at the*
502 *right) and Sections 2 and 4 based on Bayesian modelling (shaded).*

503 In comparison to the original VT-99 this approach results in a shift of +65 years for all marker
504 layers within Section 3 (Fig. A4 B). Thus, a basal age of $10,619 \pm 213$ cal. BP is obtained for Section
505 3.

506 The basal age of Section 3 is implemented as the anchor tie-point for the Bacon calculation of
507 Section 4 with a reduced error of 100 years to tighten both sections closer to each other. In



508 addition to the difficulties based on missing sediment within the YD, this section is the source of
509 highest counting uncertainties for VT-99. Section 4 is based on 25 radiocarbon dates and the latest
510 age estimation for the LST (Table A2). As in Section 2, we adjusted the sedimentation rate prior
511 ($= 0.94 \text{ yr/mm}$) based on VT-99 accumulation rate data (Zolitschka et al., 2000). The Bacon
512 software suggests a segment length of 30 mm that we applied. The resulting model covers an age
513 range from 10,663 [min.: 10,457, max.: 10,864] to 14,485 [min.: 14,287, max.: 14,721] cal. BP at
514 12.93 m (Fig. A3D, Section 4).

515 If all sections are merged, the continuous age-depth relationship forming Model D (Fig. 5) consists
516 of 63% VT-99 ages and 37% Bacon modelled ages with in total 80 missing years between the
517 sections, as it is not possible to determine the exact start and end age of the models. This
518 segmented and parameter-based integration model results in a maximum age of 14,485 [min.:
519 14,287, max.: 14,721] cal. BP (at 12.93 m) with a mean age uncertainty of 229 years, which is the
520 smallest of all four tested models. The maximum age range is 447 years at 11.09 m depth and thus
521 considerably smaller compared to those of Models A to C (Table A6).

522 **3.2.4 Comparison of model output with the isochrones UMT and** 523 **LST and the YD biozone**

524 The tephra layers of UMT and LST have been identified for sediments from Holzmaar and
525 Meerfelder Maar (Brauer et al., 1999). The varve age of 11,000 VT-99 for UMT was derived from
526 the Holzmaar chronology (Zolitschka, 1998b), while the YD hiatus of this site did not allow any
527 calendar-year estimation for LST. As no such hiatus exists between these two isochrones at
528 Meerfelder Maar, the age for the LST was derived as 1880 varve years older than UMT, i.e. as
529 12,880 VT-99. A recent study presents a new and 126 years older age for the LST (Reinig et al.,
530 2021). This age of 13,006 cal. BP was implemented for the calculation of Models A-D.

531 When we compare all models, the age estimations for UMT and LST are close to the published ages
532 with the UMT dated ca. 20-50 years earlier and thus matches well within the 95% confidence
533 interval (Table A6). Due to the new age of LST, the distances between both isochrones vary from
534 2030 (Model D) to 2057 (Model C) years, which is 150-177 years more than counted for
535 Meerfelder Maar.

536 The main differences occur in prediction of the end of the YD that defines the transition to the
537 Holocene. The rapid cooling and subsequent warming left behind easy to recognize traces in many
538 European lake records increasing the comparability between sites. The entire YD is not covered
539 by HZM19 due to a technical gap. Nevertheless, we are able to estimate depth and time range
540 based on detailed pollen investigations (Leroy et al., 2000). Using VT-99, Leroy et al. (2000) date
541 the onset of the YD, i.e. the Allerød/Younger Dryas transition (AL/YD) to 12,606 VT-99 and the



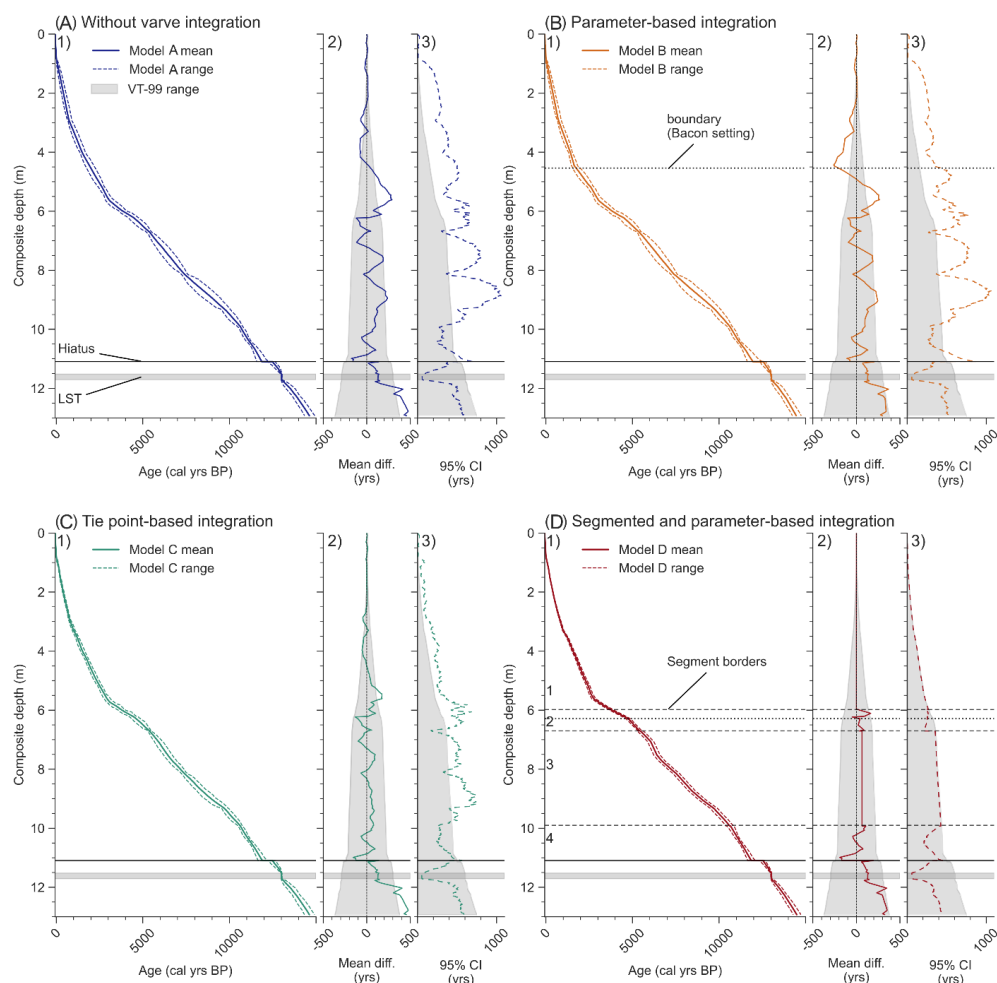
542 Younger Dryas/Preboreal (YD/PB) transition to 11,632 VT-99 with a 320 years hiatus at 12,025
543 VT-99. For HZM19 these boundaries occur at 10.88 m (YD/PB), at 11.26 m (AL/YD) and the hiatus
544 at 11.11 m (Fig. 6).

545 All model runs predict a YD duration in the range of 1012 (Model C) to 1073 (Model D) years,
546 which is longer than the 974 years given by VT-99 (Table A6). However, the predicted times are
547 closer to its duration counted for Meerfelder Maar (1080 years) (Brauer et al., 1999) or the even
548 longer time spans detected for Lake Gosciaz (1150 years) (Bonk et al., 2021)..

549 Moreover, the YD transition has been predicted within the 95% confidence interval comparable
550 to VT-99 (Table A6) and to the Meerfelder Maar record. Only the AL/YD transition varies between
551 12,694 (Model C) and 12,737 (Model B) cal. BP and, thus, is predicted earlier than for VT-99
552 (12,606 VT-99). However, this age range still covers the age estimations from Lake Gosciaz
553 (12,620 [min.: 12,389, max.: 12,753] cal. BP) and Meerfelder Maar (12,680 [min.: 12,640, max.:
554 12,720] cal. BP). In difference, the YD/PB transition varies between 11,655 (Model D) and 11,723
555 (Model B) cal. BP, which is slightly earlier than estimated by Meerfelder Maar (11,600 [min.:
556 11,570, max.: 11,630] cal. BP) and much earlier than the age estimation for Lake Gosciaz (11,470
557 [min.: 11,264, max.: 11,596] cal. BP). These discrepancies between the boundaries of the YD
558 biozone obtained by VT-99 and those obtained by the model runs are probably related to the new
559 and 126-year older age for the LST, which is included with all models. Thus, age discrepancies are
560 attenuating towards the UMT with 110 years at the AL/YD transition and 57 years at the YD/PB
561 transition.

562 **3.2.5 Comparison of model output with VT-99**

563 The comparison of all presented models differs in means and accuracies of predicted ages along
564 the core (Fig. 6A1; B1; C1; D1), which becomes more evident in comparison with VT-99 (Fig.
565 6A2,3; B2,3; C2,3; D2,3). These differences in mean modelled age and mean VT-99 age vary in
566 direction and amplitude (Fig. 6A2; B2; C2; D2). The largest age differences during the Holocene
567 occur in Model A and B with up to 300 years between 4 and 6 m depth (Fig. 6A2; B2). The defined
568 boundary in Model B results in large differences within the boundary area, predicting much
569 younger ages than VT-99. Due to the small cumulative counting uncertainty of VT-99 in the upper
570 part of the profile, the mean of Model B outranges the VT-99 error in most sections above 6 m (Fig.
571 6B2).



572

573 *Figure 6: Results of Models A, B, C, D plotted against composite depth (1), compared to VT-99 as the difference of mean ages*
574 *(Model mean – VT-99 mean) (2) and plotted vs. VT-99 confidence intervals (CI) (3).*

575 The approach used for Model C reduces the difference between VT-99 and the model, probably a
576 result of increased dating density (Fig. 6C2). This approach also leads to less over- and
577 underestimations of the model's mean age and the VT-99 age range (Fig. 6C2). Only the segmented
578 insertion of VT-99 in model D results in comparable ages during the Holocene (Fig. 6D2)

579 In the Late Glacial part below 11 m, all models produce ages constantly older than VT-99 (Fig. 6A2,
580 B2, C2, D2). The age differences are even higher (up to 477 years), when the Bacon prior for
581 accumulation rates was not adjusted to VT-99 (Fig. 6A2, C2). In the other cases the maximum age
582 differences are 369 and 354 years for Model B and D, respectively (Fig. 6B2, D2). Hajdas et al.
583 (2000) already observed a shift between the varve ages of radiocarbon dated samples and
584 calibrated ages using the INTCAL98 calibration curve (Stuiver et al., 1998) and discuss the



585 difference using the LST age estimation from Meerfelder Maar (12,880 VT). However, no
586 adjustment has been made to fit the VT-99 ages to the calibration curve. With the LST dated to
587 13,006 \pm 9 cal. BP (Reinig et al., 2021) and the use of the INTCAL20 calibration curve, an
588 underestimation of VT-99 compared to the calibration curve is still existing (Fig. A2). Therefore,
589 a correction of ages older than 12,800 cal. BP is needed to ensure comparability of HZM19 to other
590 sites.

591 In order to find the best method to transfer VT-99 to HZM19 and to improve the chronology by
592 using Bayesian modelling, a closer look to each model's accuracy is necessary (Fig. 6A3, B3, C3,
593 D3). In comparison to the cumulative VT-99 counting error, Models A and B show maximum
594 differences in age uncertainties up to +655 and +665 years, respectively (Table A6). Especially
595 below 9.82 m, both models predict ages with larger uncertainties than the estimated counting
596 error for VT-99, particularly with increasing distance to radiocarbon dated levels. Therefore, no
597 improvement in accuracy of age estimations is observed when using the parameter-based
598 approach (Model B).

599 The tie point-based Model C also predicts larger uncertainties than VT-99 below 9.82 m (Fig. 6C),
600 whereas the overall difference of the age range is reduced to a mean of 47 years with a maximum
601 of +401 years (Table A6). Only the segmented and parameter-based Model D shows no
602 significantly enlarged age uncertainties and an overall improved mean age range as it adapts the
603 cumulative error of the varve chronology in Sections 1 and 3 (Table A6). The overall improvement
604 occurs in Sections 2 and 4, which is the result of more detailed prior settings for the model run.
605 However, all age models result in more accurate age estimations in the Late Glacial part, where
606 the cumulative counting error is higher and radiocarbon dating sampling is dense. But still we see
607 that Models C and D perform best within this section, as they predict ages with constantly lower
608 uncertainty ranges than VT-99. This is in contrast to the other models, which show increased and
609 therefore larger uncertainties at a depth of ca. 11 m. As we calculate this section in Model D with
610 the same data like for Model A and B, we assume that the better adjustment of the sedimentation
611 rate mean prior of Model D influences the model's accuracy. In terms of accuracy, there are no
612 general improvements in calculating a single model for the entire record, but improvements are
613 realised by adjusting the priors in a more detailed way.

614 **4. Evaluation of the different varve integration techniques**

615 All models predict convincing age estimations for the isochrones of LST and UMT, whereas the
616 prediction of the YD between both isochrones remains somewhat ambiguous, due to a
617 documented hiatus and too few radiocarbon ages being available for this biozone.



618 In terms of accuracy and precision, the varve-integration technique applied in Model D,
619 introduced by Bonk et al. (2021), results in most convincing age estimations for HZM19. Especially
620 in terms of accuracy, none of the completely Bayesian modelled age-depth relationships improved
621 the small age uncertainties of VT-99 in the upper part. Only in sections with markedly higher
622 radiocarbon sampling density or in sections with high varve counting uncertainty the Bacon
623 models perform better and result in more accurate age estimations than VT-99.

624 In comparison, Model B shows nearly no improvement over the approach without varve
625 integration (Model A). The reason is probably the low-resolution definition of sedimentation rate
626 changes (boundaries) for HZM19, which does not reflect the complex accumulation history. Also
627 Vandergoes et al. (2018) reject this integration model. We suggest that this form of varve
628 integration is more useful for less complex and for shorter sediment profiles.

629 Better results are observed applying Model C, which is actually the easiest to apply. The accuracy
630 is improved compared to Models A and B as the dating density increases significantly. Based on
631 the Bayesian approach, this leads to smaller age ranges as higher uncertainties occur with
632 increasing distances to dated levels. The resulting mean age is more constrained by VT-99. The
633 accuracy might be improved by additional adjustments of the sedimentation-rate prior (here:
634 based on VT-99). However, varve ages inserted as tie points are included with normal distribution.
635 Therefore, they should not be interpreted as independent measurements with non-normal
636 distributed PDFs. Bayesian statistics could weight tie points too much when they are included too
637 densely. Therefore, this approach should be interpreted with care.

638 The best result in precision and especially accuracy is achieved by the segmented and parameter-
639 based Model D. This approach is the most challenging, but makes advantage of both, the high
640 accuracy of varve counting and the Bayesian approach for densely radiocarbon dated sections.
641 The main difference to the other models is that Model D replaces the sections of lower dating
642 accuracy with modelled ages that incorporate varve information and radiocarbon measurements,
643 which result in a much better performance.

644 For upcoming geochemical and geophysical studies of the HZM19 record, we will use Model D. As
645 parts of VT-99 (63%) are included in the new chronology, we will refer to it as chronology “VT-
646 22”, which delivers highly accurate age estimations for each depth of the sediment profile HZM19.
647 Altogether, this will improve the comparability of the Holzmaar record with other sites.

648 5. Conclusion

649 As limnogeological and varve studies proceed, new techniques for sediment analysis develop.
650 Thus, previous studies can be improved by reinvestigation. However, many of the previously
651 studied sediment cores are not available for analysis anymore. We expect such cases to happen



652 more frequently in the future. Rarely, the rather time-consuming and expensive chronological
653 studies, especially if the counting of varves is involved, will be funded a second time. This
654 increases the need for finding best ways to adapt varve chronologies obtained during previous
655 studies and to transfer them efficiently and precisely to new sediment cores.

656 For the well-dated Holzmaar record, we tested three different approaches for the integration of
657 varve counting and radiocarbon dating using Bayesian modelling and applied them to the new
658 composite profile from Holzmaar (HZM19). We conclude that all models result in accurate and
659 precise age estimations. However, with higher dating density and more prior settings used to
660 adjust the Bacon model runs, the model output is enhanced. This is confirmed by results of Model
661 D, which improved and corrected the age estimations considerably. In contrast, Models B and C
662 show nearly no improvement over VT-99 just like the output of Model A without varve integration.

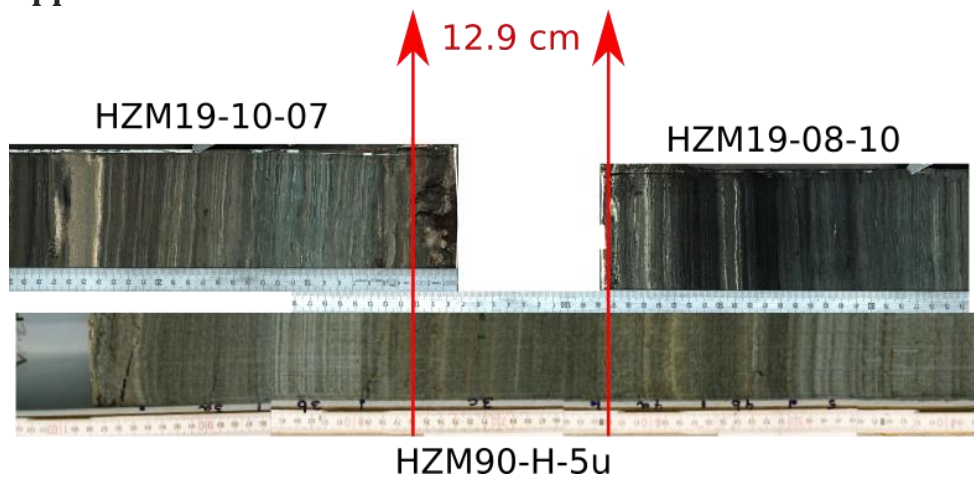
663 Multiple varve counting is still one of the best approaches of building a reliable chronology for
664 lacustrine sediment archives. However, the occurrence of hiatus or errors in varve counts lead to
665 larger uncertainties with increasing depth that need to be corrected by using independent dating
666 techniques. Therefore, if varve and radiocarbon data are available, like it is the case for Holzmaar,
667 the transfer of both to form a new and integrating chronology is the best option.

668 For this study of varve integration, we use Bacon. The parameter adjustment of Bacon is complex
669 and especially beginners have problems to understand each single parameter and the effect it has
670 on model results. We compare different models and settings, which helps to decide selecting the
671 best suited approach. and to consider the parameters that have to be adjusted. After all, we suggest
672 to increase the independent dating density and to adjust prior settings as detailed as possible to
673 gain a more precise chronology for the varve-integration attempt.

674 Optimizing the Holzmaar chronology is the first step in order to provide a precise and robust age-
675 depth model for upcoming and high-resolution multi-proxy investigations to unveil all the
676 environmental details recorded by the varved sediment archive of Holzmaar.



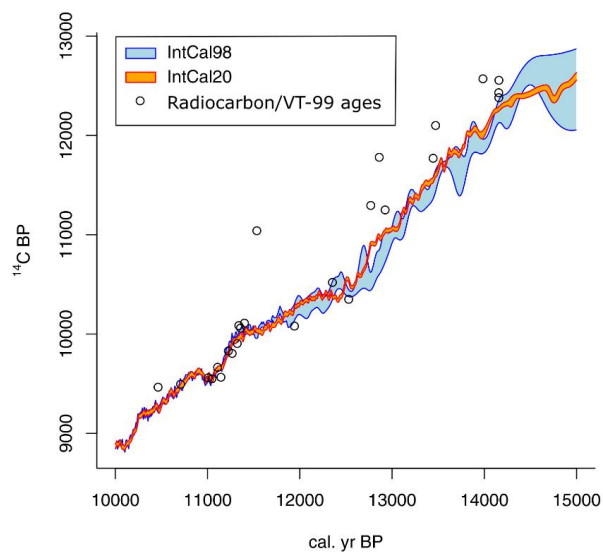
677 **Appendix**



678

679 *Figure A1: Determination of the technical gap for HZM19 during the YD. This gap exists between sections HZM19-10-07*
680 *and HZM19-08-10 and is bridged by section HZM90-H5u from an earlier coring campaign.*

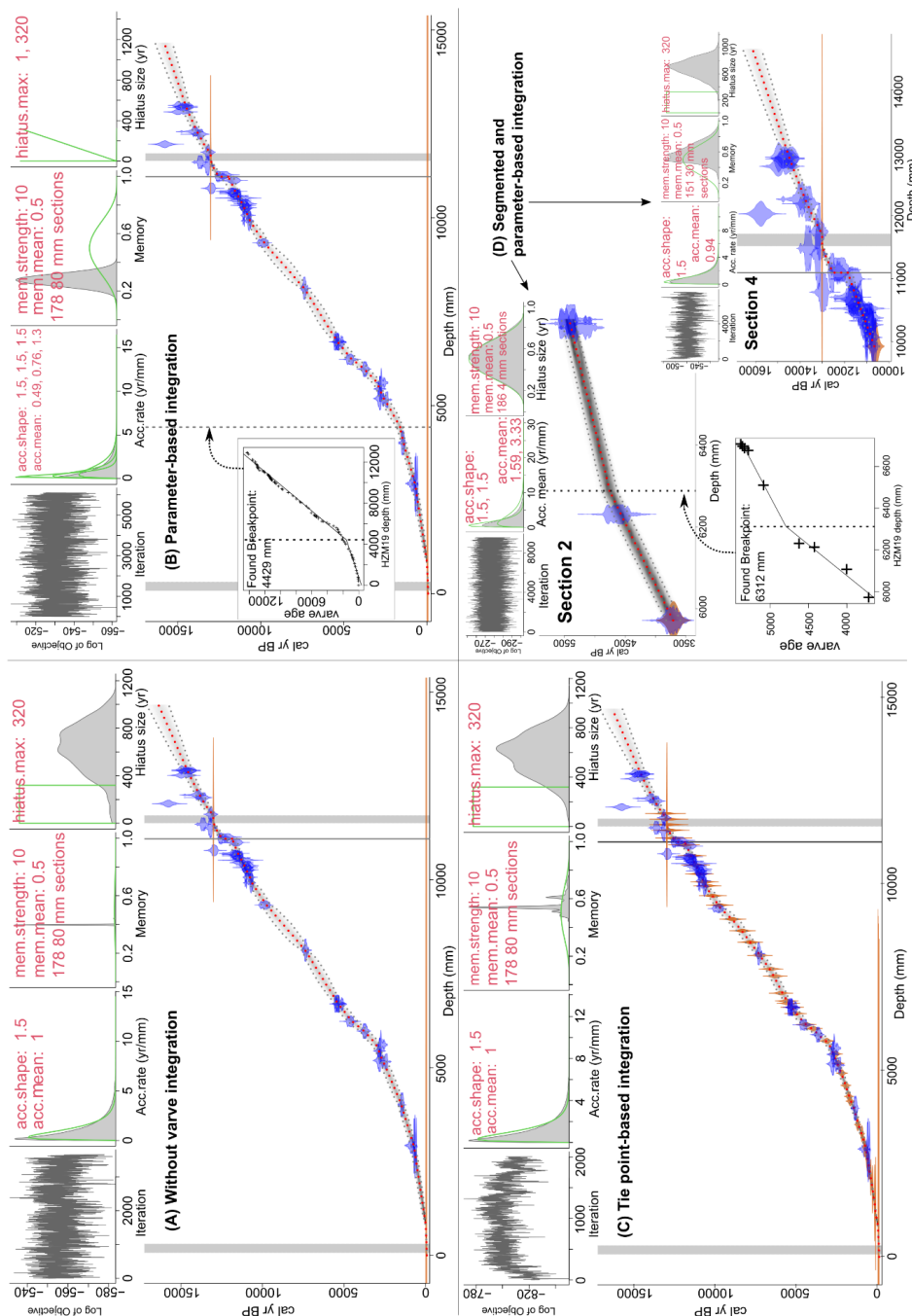
681



682

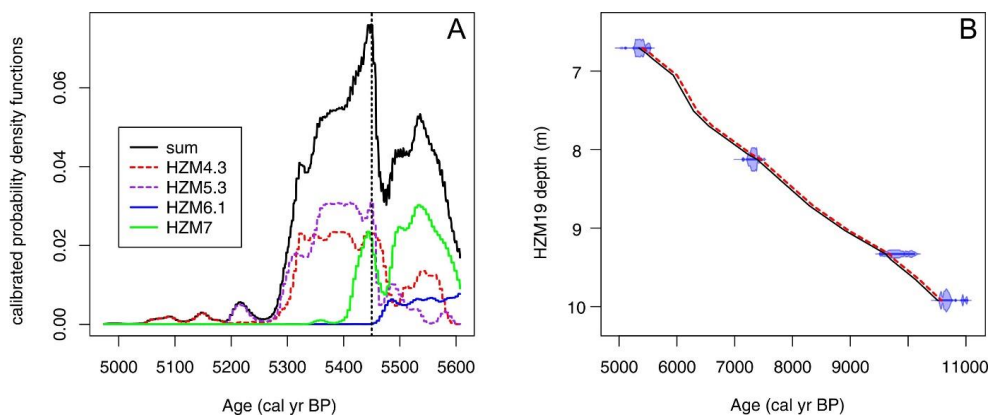
683 *Figure A2: Radiocarbon ages vs. Intcal98 and Intcal20 calibrated ages between 10,000 and 15,000 cal BP. Black circles*
684 *show radiocarbon ages from Holzmaar vs. VT-99 age. An underestimation of these ages occurs after 12,500 cal BP, where*
685 *VT-99 seems to be too young.*

686



687

688 Figure A3: Bacon output for Model A, B, C and D (sections 2 and 4. Each output with indicator panels from top left to right:
 689 MCMC iterations, prior (green) and posterior (grey) for accumulation rate distribution, memory and hiatus with defined
 690 settings in red. Main panel: model with calibrated radiocarbon date probabilities (blue), tie-points with normal distribution
 691 (orange) and the posterior age-depth model with mean (red dotted line) and 95% confidence intervals (gray dotted line).
 692 Vertical gray lines (from left to right): slump event, defined hiatus and Laacher See Tephra. In additional panels of Models
 693 B and D2 boundaries indicating major changes in accumulation rate are provided as vertical dotted lines.



694

695 *Figure A4: Calculations for the floating VT-99 chronology of Model D, section 3. A: Calculation of shift based on calibrated*
696 *probability density functions of each radiocarbon sample within this section. The maximum summed probability occurs at*
697 *5450 cal BP. B: Original VT-99 (black) vs. floating VT-99 (+65 years, red dotted) with calibrated radiocarbon samples*
698 *plotted vs. depth.*

699



700 *Table A1: Error (1 sigma) estimations for different varve quality periods for the Holzmaar record (Zolitschka, 1998b),*
701 *updated from VT-95 to VT-99.*

Varve quality period	VT-99 (duration in years)	Error
A	0 – 2800	±4.0 %
B	2800 – 5300	±2.6 %
C	5300 – 11,600	±0.7 %
D	11,600 – 14,158	±5.9 %
Entire record	0 – 14,158	±2.5 %

702

703

704



705 *Table A2: Marker layers (in italics) and radiocarbon dates (Hajdas et al., 2000, 1995 plus one unpublished radiocarbon*
 706 *date) vs. composite depth of HZM19. The calibrated median ¹⁴C age is calculated using OxCal with the IntCal20 calibration*
 707 *curve. Inconsistent calibrated ages are shown in brackets.*

Marker layer and ¹⁴ C sample ID	HZM19 depth (m)	VT-99 Age (cal BP)	VT-99 cumulative ±1σ error (yrs)	¹⁴ C age (BP)	¹⁴ C ±1σ error (yrs)	Calibrated ¹⁴ C median age (cal BP)	¹⁴ C ±1σ error (yrs)
<i>ML-36/1</i>	1.16	141	6				
<i>ML-36</i>	1.45	209	8				
<i>ML-35/1</i>	1.81	334	13				
<i>ML-35</i>	2.12	442	18				
<i>ML-34</i>	2.44	572	23				
<i>ML-33/2</i>	2.62	657	26				
<i>ML-33/1</i>	2.69	685	27				
HZM-1.1	2.90	796	32	685	40	644	41
HZM-1.2	2.91	802	32	795	40	708	29
HZM-1.3	2.93	810	32	975	90	869	94
<i>ML-33</i>	2.94	819	33				
<i>ML-32</i>	3.29	985	39				
<i>ML-31/1</i>	3.54	1248	50				
HZM-2.2+3	4.01	1569	63	1565	55	1451	57
<i>ML-31</i>	4.17	1710	68				
<i>ML-30</i>	4.29	1789	72				
<i>ML-29</i>	4.59	1984	79				
<i>ML-28</i>	4.91	2219	89				
HZM-3.1	5.16	2433	97	2405	60	2469	112
<i>ML-27</i>	5.17	2449	98				
HZM-3.3*	5.19	2450	98	2750	60	(2850)	66
<i>ML-26</i>	5.43	2593	104				
HZM-23*	5.45	2595	104	2720	60	(2826)	58
HZM-24	5.61	2754	110	2620	65	2743	101
<i>ML-25/1</i>	5.77	3147	121				
HZM-25	5.97	3704	136	3465	70	3730	96
<i>ML-25</i>	6.11	3992	143				
<i>ML-24</i>	6.21	4420	154				
HZM-26*	6.23	4616	159	4100	90	4624	127
<i>ML-23</i>	6.51	5083	171				
<i>ML-22</i>	6.68	5286	177				
HZM-4.1	6.69	5334	177	4575	65	5243	131
HZM-4.2	6.70	5359	177	4730	70	5462	85
HZM-4.3	6.71	5385	178	4675	70	5409	95
<i>ML-21</i>	6.78	5520	179				
<i>ML-20</i>	6.84	5619	179				
<i>ML-19</i>	7.05	5977	182				
<i>ML-18/2</i>	7.51	6328	184				
<i>ML-18/1</i>	7.70	6590	186				
<i>ML-18</i>	8.06	7274	191				
HZM-5.3	8.13	7428	192	6455	70	7363	68
<i>ML-17/3</i>	8.42	7870	195				
<i>ML-17/2</i>	8.72	8338	198				



ML-17/1	9.03	8943	203				
HZM-6.1	9.33	9649	207	8800	95	9851	170
ML-17	9.40	9746	208				
ML-16	9.66	10169	211				
HZM-7	9.92	10464**	213	9465	45	10705	130
ML-15	9.92	10554	214				
ML-14	10.03	10681	215				
HZM-8	10.07	10708	215	9495	55	10773	148
ML-13	10.24	10999	217				
HZM-9 (UMT)	10.25	11008	217	9560	49	10923	121
HZM-40	10.27	11048	217	9550	80	10901	148
HZM-41	10.33	11109	218	9665	100	10998	154
HZM-42	10.38	11145	218	9565	100	10912	160
HZM-43	10.46	11226	219	9830	100	11264	178
ML-12	10.48	11232	219				
HZM-44	10.52	11267	219	9805	190	11243	329
HZM-45	10.59	11322	219	9905	80	11357	138
HZM-46	10.64	11357**	219	10060	80	11584	159
HZM-10.1	10.67	11339**	219	10085	80	11630	165
HZM-47	10.70	11400	220	10110	110	11680	231
ML-11	10.73	11453	220				
HZM-48	10.78	11534	221	11040	140	(12959)	120
HZM-50	10.99	11942	241	10080	110	11628	214
ML-9	11.02	11943	241				
HZM-12	11.10	12354	266	10520	90	12509	181
HZM-51	11.14	12530	276	10350	90	12203	194
ML-8	11.20	12578	279				
HZM-13*	11.38	12769	290	11295	85	(13197)	74
ML-7	11.41	12778	291				
HZM-14*	11.48	12861	296	11780	100	(13647)	112
ML-6	11.56	12880	297				
ML-5	11.70	12880	297				
HZM-30	11.74	12925	299	11250	110	13158	109
ML-4	11.86	13087	309				
HZM-16*	12.03	13130	311	13140	140	(15766)	212
HZM-32	12.19	13445	330	11770	135	13642	150
HZM-17	12.26	13472	332	12100	110	13984	183
ML-3	12.40	13646**	339				
HZM-35	12.78	13985	362	12570	130	14858	286
ML-2	12.86	14152**	369				
HZM-18	12.90	14156	372	12430	110	14586	249
ML-1	12.90	14156**	372				
HZM-100***	12.92	14157	372	12380	85	14492	228
HZM-19	12.93	14158	372	12555	80	14879	221

708

709

710

711

712

713

* Dates described to contain reworked organic material or being fractionated during graphitization (see Hajdas et al., 1995).

** VT-99 dates excluded from modelling due to inconsistencies in documentation.

*** unpublished radiocarbon age (KIA-1460)



714 *Table A3: Core section depths of the composite profile HZM19 with resulting composite end depths for each core.*

Core section	From [mm]	To [mm]	Length [mm]	Composite core section end depth [mm]
HZM19_07_01	138	800	662	662
HZM19_08_01	305	755	451	1113
HZM19_07_02	243	924	681	1794
HZM19_08_02	380	839	459	2254
HZM19_07_03	229	912	683	2936
HZM19_08_03	375	714	339	3275
HZM19_07_04	243	800	557	3833
HZM19_08_04	235	994	759	4592
HZM19_10_01	90	913	823	5415
HZM19_08_05	630	930	299	5715
HZM19_10_02	183	877	693	6409
HZM19_08_06	596	957	361	6770
HZM19_10_03	87	827	740	7510
HZM19_08_07	562	971	409	7919
HZM19_10_04	179	870	691	8611
HZM19_08_08	641	967	326	8937
HZM19_10_05	137	859	722	9659
HZM19_11_06	395	655	260	9919
HZM19_08_10	35	974	939	10859
Technical gap			129	10988
HZM19_10_07	30	810	780	11768
HZM19_11_07	710	1012	302	12071
HZM19_10_08	72	902	830	12902
HZM19_11_08	326	1245	919	13822
HZM19_07_17	100	920	820	14643

715

716

717



718 Table A4: Core section and composite depths of lithozones H1 to H12 for HZM19

Lithozone	From		To		Biozone	Human phase
	Section depth [mm]	Composite depth [mm]	Section depth [mm]	Composite depth [mm]		
H12	HZM19_07_01	138	HZM19_08_01	700	Subatlantic	Last century
H11	HZM19_08_01	700	HZM19_08_03	520	Subatlantic	Middle Ages / Little Ice Age
H10	HZM19_08_03	520	HZM19_08_04	710	Subatlantic	Migration Period / Early Middle Ages
H9	HZM19_08_04	710	HZM19_08_05	750	Subatlantic	Iron Age / Roman Period
H8	HZM19_08_05	750	HZM19_10_05	480	Subboreal/Atlantic	
H7	HZM19_10_05	480	HZM19_11_06	588	Boreal	
H6	HZM19_11_06	588	HZM19_08_10	140	Preboreal	
H5	HZM19_08_10	140	HZM19_08_10	860	Preboreal	
H4	HZM19_08_10	860	HZM19_08_10	970	Preboreal	
H3	HZM19_08_10	970	HZM19_10_07	300	Younger Dryas	
H2	HZM19_10_07	300	HZM19_10_08	859	Bölling/Alleröd	
H1	HZM19_10_08	860	HZM19_07_17	920	Pleniglacial (Late Weichselian)	



719 *Table A5: Additional dates for the HZM19 chronology with composite depths, ages (cal. BP) and errors used for Bacon*
720 *calculations. LST age with error is from Reinig et al. (2020).*

Event	HZM19 comp. depth (cm)	Age (cal. BP)	error
Sediment surface	0.00	-69	1
Chernobyl accident	47.20*	-36	1
Maximum atomic bomb tests	67.20*	-13	1
First atomic bomb tests	79.20*	0	1
Laacher See Tephra	1160.00	13,006	9

721 *22 cm subtracted due to slump event documented by Pb-210 data.

722



723 *Table A6: Age estimations for VT-99 and Models A-D with their 95% confidence intervals in brackets for Ulmener Maar*
 724 *Tephra (UMT), Younger Dryas/Preboreal-transition (YD/PB), YD duration, Allerød/Younger Dryas-transition (AL/YD),*
 725 *predicted YD hiatus with duration and position, Laacher See Tephra (LST), Maximum model age at 12.93 m with its mean*
 726 *and maximum age ranges and position of the maximum age range and maximum difference between VT-99 and each of*
 727 *the model ranges.*

Chronology	VT-99	A	B	C	D
Age of	10999	10961	10965	10952	10981
UMT	[10782, 11216]	[10784, 11090]	[10787, 11093]	[10788, 11067]	[10829, 11088]
YD/PB	11632	11674	11723	11682	11655
transition		[11461, 11965]	[11486, 12070]	[11494, 11913]	[11499, 11845]
YD	974	1038	1014	1012	1073
duration					
AL/YD	12606	12712	12737	12694	12728
transition		[12517, 12880]	[12562, 12880]	[12475, 12869]	[12595, 12838]
Duration of YD hiatus	320	623	603	583	686
End of YD hiatus	12025	11863	11952	11901	11854
		[11571, 12269]	[11623, 12502]	[11646, 12207]	[11651, 12098]
Age of	12880	13010	13010	13009	13011
LST	[12583, 13177]	[12984, 13042]	[12985, 13043]	[12984, 13037]	[12984, 13043]
Maximum model age	14158	14615	14456	14614	14485
(at 12.93 m)	[13786, 14530]	[14339, 14926]	[14236, 14749]	[14332, 14919]	[14287, 14721]
Mean	282	468	456	329	229
age range					
Maximum age range	744	1056	1064	749	447
Max. age range position (m)	12.93	8.86	8.78	9.18	11.09
Maximum difference to VT-99 age range	0	655	665	401	0

728

729



730 **Data Availability**

731 The results of the different age-depth models carried out for the lacustrine sediment record
732 from Holzmaar are accessible via the PANGAEA data archiving and publication system at
733 <https://doi.org/10.1594/PANGAEA.xxxxxx>.

734 **Author contributions**

735 SB and BZ conducted the fieldwork and conceptualized the study. SB described and sampled the
736 sediment, modified and run the Bayesian age-depth models, visualized the data and drafted the
737 first version of the manuscript. WT measured and interpreted lead and cesium data. All authors
738 contributed to the writing and to revising of the manuscript.

739 **Competing interests**

740 The contact author declares that neither she nor her co-authors have any competing interests.

741 **Disclaimer**

742 **Acknowledgments**

743 We like to thank Christian Ohlendorf, Rafael Stiens and An-Sheng Lee for participating in the
744 coring campaign of 2019 and also for subsequent help with core opening, sediment preparations
745 and scanning in the GEOPOLAR lab. Furthermore, we want to thank Maarten Blaauw, Arne
746 Ramisch and Alicja Bonk for helpful discussions.

747 **References**

- 748 Anderson, R. Y. and Dean, W. E.: Lacustrine varve formation through time, *Palaeogeogr. Palaeocl.*,
749 62, 215–235, [https://doi.org/10.1016/0031-0182\(88\)90055-7](https://doi.org/10.1016/0031-0182(88)90055-7), 1988.
- 750 Baier, J., Lücke, A., Negendank, J. F. W., Schleser, G.-H., and Zolitschka, B.: Diatom and
751 geochemical evidence of mid- to late Holocene climatic changes at Lake Holzmaar, West-Eifel
752 (Germany), *Quatern. Int.*, 113, 81–96, [https://doi.org/10.1016/S1040-6182\(03\)00081-8](https://doi.org/10.1016/S1040-6182(03)00081-8), 2004.
- 753 Blaauw, M.: Methods and code for ‘classical’ age-modelling of radiocarbon sequences, *Quat.*
754 *Geochronol.*, 5, 512–518, <https://doi.org/10.1016/j.quageo.2010.01.002>, 2010.
- 755 Blaauw, M. and Christen, J. A.: Flexible paleoclimate age-depth models using an autoregressive
756 gamma process, *Bayesian Anal.*, 6, 457–474, <https://doi.org/10.1214/11-BA618>, 2011.
- 757 Blaauw, M., Christen, J. A., Bennett, K. D., and Reimer, P. J.: Double the dates and go for Bayes —
758 Impacts of model choice, dating density and quality on chronologies, *Quaternary Sci. Rev.*, 188,
759 58–66, <https://doi.org/10.1016/j.quascirev.2018.03.032>, 2018.



- 760 Blaauw, M., Christen, J. A., Lopez, M. A. A., Vazquez, J. E., V, O. M. G., Belding, T., Theiler, J., Gough,
761 B., and Karney, C.: rbacon: Age-Depth Modelling using Bayesian Statistics, CRAN [code], 2021.
- 762 Bonk, A., Müller, D., Ramisch, A., Kramkowski, M. A., Noryskiewicz, A. M., Sekudewicz, I.,
763 Gąsiorowski, M., Luberd-Durnaś, K., Słowiński, M., Schwab, M., Tjallingii, R., Brauer, A., and
764 Błaszczewicz, M.: Varve microfacies and chronology from a new sediment record of Lake Gościąg
765 (Poland), *Quaternary Sci. Rev.*, 251, 106715, <https://doi.org/10.1016/j.quascirev.2020.106715>,
766 2021.
- 767 Brauer, A.: Weichselzeitliche Seesedimente des Holzmaars - Warvenchronologie des
768 Hochglazials und Nachweis von Klimaschwankungen, Ph.D. thesis, Universität Trier, *Documenta*
769 *naturae*, 85, 1–210, 1994.
- 770 Brauer, A., Hajdas, I., Negendank, J. F. W., Rein, B., Vos, H., and Zolitschka, B.: Warvenchronologie
771 - eine Methode zur absoluten Datierung und Rekonstruktion kurzer und mittlerer solarer
772 Periodizitäten, *Geowissenschaften*, 12, 325–332, 1994.
- 773 Brauer, A., Endres, C., Günter, C., Litt, T., Stebich, M., and Negendank, J. F. W.: High resolution
774 sediment and vegetation responses to Younger Dryas climate change in varved lake sediments
775 from Meerfelder Maar, Germany, *Quaternary Sci. Rev.*, 18, 321–329,
776 [https://doi.org/10.1016/S0277-3791\(98\)00084-5](https://doi.org/10.1016/S0277-3791(98)00084-5), 1999.
- 777 Brooks, S. P. and Gelman, A.: General Methods for Monitoring Convergence of Iterative
778 Simulations, *J. Comput. Graph. Stat.*, 7, 434–455,
779 <https://doi.org/10.1080/10618600.1998.10474787>, 1998.
- 780 Büchel, G.: Maars of the Westeifel, Germany, in: *Paleolimnology of European Maar Lakes*, edited
781 by: Negendank, J. F. W. and Zolitschka, B., Springer, Berlin, Heidelberg, 1–13,
782 <https://doi.org/10.1007/BFb0117585>, 1993.
- 783 De Geer, G.: A geochronology of the last 12,000 years., *Eleventh International Geological*
784 *Congress, Stockholm*, 1, 241–253, 1912.
- 785 Dean, W. E., Bradbury, J. P., Anderson, R. Y., and Barnosky, C. W.: The Variability of Holocene
786 Climate Change: Evidence from Varved Lake Sediments, *Science*, 226, 1191–1194,
787 <https://doi.org/10.1126/science.226.4679.1191>, 1984.
- 788 García, M. L., Birlo, S., and Zolitschka, B.: Paleoenvironmental changes of the last 16,000 years
789 based on diatom and geochemical stratigraphies from Holzmaar (West-Eifel Volcanic Field,
790 Germany), *Quaternary Sci. Rev.*, accepted manuscript,
791 <https://doi.org/10.1016/j.quascirev.2022.107691>, 2022.
- 792 Goslar, T., Kuc, T., Ralska-Jasiewiczowa, M., Różanski, K., Arnold, M., Bard, E., van Geel, B., Pazdur,
793 M., Szeroczyńska, K., Wicik, B., Więckowski, K., and Walanus, A.: High-resolution lacustrine
794 record of the late glacial/holocene transition in central Europe, *Quaternary Sci. Rev.*, 12, 287–
795 294, [https://doi.org/10.1016/0277-3791\(93\)90037-M](https://doi.org/10.1016/0277-3791(93)90037-M), 1993.
- 796 Hajdas, I., Zolitschka, B., Ivy-Ochs, S. D., Beer, J., Bonani, G., Leroy, S. A. G., Negendank, J. W.,
797 Ramrath, M., and Suter, M.: AMS radiocarbon dating of annually laminated sediments from lake
798 Holzmaar, Germany, *Quaternary Sci. Rev.*, 14, 137–143, [https://doi.org/10.1016/0277-3791\(94\)00123-S](https://doi.org/10.1016/0277-3791(94)00123-S), 1995.
- 800 Hajdas, I., Bonani, G., and Zolitschka, B.: Radiocarbon Dating of Varve Chronologies: Soppensee
801 and Holzmaar Lakes after Ten Years, *Radiocarbon*, 42, 349–353,
802 <https://doi.org/10.1017/S0033822200030290>, 2000.



- 803 Hajdas-Skowronek, I.: Extension of the radiocarbon calibration curve by AMS dating of
804 laminated sediments of Lake Soppensee and Lake Holzmaar, Ph. D thesis, ETH Zurich,
805 <https://doi.org/10.3929/ETHZ-A-000916163>, 1993.
- 806 Haslett, J. and Parnell, A.: A simple monotone process with application to radiocarbon-dated
807 depth chronologies, *J. R. Stat. Soc. C.-Appl.*, 57, 399–418, [https://doi.org/10.1111/j.1467-](https://doi.org/10.1111/j.1467-9876.2008.00623.x)
808 [9876.2008.00623.x](https://doi.org/10.1111/j.1467-9876.2008.00623.x), 2008.
- 809 Kienel, U., Schwab, M. J., and Schettler, G.: Distinguishing climatic from direct anthropogenic
810 influences during the past 400 years in varved sediments from Lake Holzmaar (Eifel, Germany),
811 *J. Paleolimnol.*, 33, 327–347, <https://doi.org/10.1007/s10933-004-6311-z>, 2005.
- 812 Lacourse, T. and Gajewski, K.: Current practices in building and reporting age-depth models,
813 *Quaternary Res.*, 96, 28–38, <https://doi.org/10.1017/qua.2020.47>, 2020.
- 814 Leroy, S. A. G., Zolitschka, B., Negendank, J. F. W., and Seret, G.: Palynological analyses in the
815 laminated sediment of Lake Holzmaar (Eifel, Germany): duration of Lateglacial and Preboreal
816 biozones, *Boreas*, 29, 52–71, <https://doi.org/10.1111/j.1502-3885.2000.tb01200.x>, 2000.
- 817 Litt, T., Schölzel, C., Köhl, N., and Brauer, A.: Vegetation and climate history in the Westeifel
818 Volcanic Field (Germany) during the past 11 000 years based on annually laminated lacustrine
819 maar sediments, *Boreas*, 38, 679–690, <https://doi.org/10.1111/j.1502-3885.2009.00096.x>,
820 2009.
- 821 Lorenz, V.: Explosive Volcanism of the West Eifel Volcanic Field/Germany, in: *Developments in*
822 *Petrology*, vol. 11, edited by: Kornprobst, J., Elsevier, 299–307, [https://doi.org/10.1016/B978-0-](https://doi.org/10.1016/B978-0-444-42273-6.50026-2)
823 [444-42273-6.50026-2](https://doi.org/10.1016/B978-0-444-42273-6.50026-2), 1984.
- 824 Lorenz, V., Lange, T., and Büchel, G.: Die Vulkane der Westeifel, *Jahresberichte und Mitteilungen*
825 *des Oberrheinischen Geologischen Vereins*, 102, 379–411,
826 <https://doi.org/10.1127/jmogv/102/0022>, 2020.
- 827 Lotter, A. F.: Absolute Dating of the Late-Glacial Period in Switzerland Using Annually Laminated
828 Sediments, *Quaternary Res.*, 35, 321–330, [https://doi.org/10.1016/0033-5894\(91\)90048-A](https://doi.org/10.1016/0033-5894(91)90048-A),
829 1991.
- 830 Lottermoser, B. G., Oberhänsli, R., Zolitschka, B., Negendank, J. F. W., Schütz, U., and Boenecke, J.:
831 Environmental geology and geochemistry of lake sediments (Holzmaar, Eifwl, Germany), in:
832 *Paleolimnology of European Maar Lakes*, vol. 49, edited by: Negendank, J. F. W. and Zolitschka,
833 B., Springer Berlin Heidelberg, Berlin, Heidelberg, 305–316,
834 <https://doi.org/10.1007/BFb0117603>, 1993.
- 835 Lücke, A., Schleser, G. H., Zolitschka, B., and Negendank, J. F. W.: A Lateglacial and Holocene
836 organic carbon isotope record of lacustrine palaeoproductivity and climatic change derived from
837 varved lake sediments of Lake Holzmaar, Germany, *Quaternary Sci. Rev.*, 22, 569–580,
838 [https://doi.org/10.1016/S0277-3791\(02\)00187-7](https://doi.org/10.1016/S0277-3791(02)00187-7), 2003.
- 839 Martin-Puertas, C., Walsh, A. A., Blockley, S. P. E., Harding, P., Biddulph, G. E., Palmer, A., Ramisch,
840 A., and Brauer, A.: The first Holocene varve chronology for the UK: Based on the integration of
841 varve counting, radiocarbon dating and tephrostratigraphy from Diss Mere (UK), *Quat.*
842 *Geochronol.*, 61, 101134, <https://doi.org/10.1016/j.quageo.2020.101134>, 2021.
- 843 Meyer, W.: Zur Entstehung der Maare in der Eifel, *Z. Dtsch. Ges. Geowiss.*, 141–155,
844 <https://doi.org/10.1127/zdgg/136/1985/141>, 1985.



- 845 Meyer, W.: *Geologie der Eifel*, 4th ed., Schweizerbart Science Publishers, Stuttgart, Germany,
846 2013.
- 847 Meyer, W. and Stets, J.: Pleistocene to Recent tectonics in the Rhenish Massif (Germany), *Neth. J.*
848 *Geosci.*, 81, 217–221, <https://doi.org/10.1017/S0016774600022460>, 2002.
- 849 Muggeo, V. M. R.: segmented: Regression Models with Break-Points / Change-Points Estimation,
850 CRAN [code], 2022.
- 851 O'Sullivan, P. E.: Annually-laminated lake sediments and the study of Quaternary environmental
852 changes — a review, *Quaternary Sci. Rev.*, 1, 245–313, [https://doi.org/10.1016/0277-](https://doi.org/10.1016/0277-3791(83)90008-2)
853 [3791\(83\)90008-2](https://doi.org/10.1016/0277-3791(83)90008-2), 1983.
- 854 Prasad, S. and Baier, J.: Tracking the impact of mid- to late Holocene climate change and
855 anthropogenic activities on Lake Holzmaar using an updated Holocene chronology, *Global*
856 *Planet. Change*, 122, 251–264, <https://doi.org/10.1016/j.gloplacha.2014.08.020>, 2014.
- 857 R Core Team: *R: A Language and Environment for Statistical Computing*, 2021.
- 858 Ramsey, C. B.: Deposition models for chronological records, *Quaternary Sci. Rev.*, 27, 42–60,
859 <https://doi.org/10.1016/j.quascirev.2007.01.019>, 2008.
- 860 Ramsey, C. B.: Bayesian Analysis of Radiocarbon Dates, *Radiocarbon*, 51, 337–360,
861 <https://doi.org/10.1017/S0033822200033865>, 2009.
- 862 Raubitschek, S., Lücke, A., and Schleser, G. H.: Sedimentation patterns of diatoms in Lake
863 Holzmaar, Germany - (on the transfer of climate signals to biogenic silica oxygen isotope
864 proxies), *J. Paleolimnol.*, 21, 437–448, 1999.
- 865 Reimer, P. J., Austin, W. E. N., Bard, E., Bayliss, A., Blackwell, P. G., Bronk Ramsey, C., Butzin, M.,
866 Cheng, H., Edwards, R. L., Friedrich, M., Grootes, P. M., Guilderson, T. P., Hajdas, I., Heaton, T. J.,
867 Hogg, A. G., Hughen, K. A., Kromer, B., Manning, S. W., Muscheler, R., Palmer, J. G., Pearson, C., van
868 der Plicht, J., Reimer, R. W., Richards, D. A., Scott, E. M., Southon, J. R., Turney, C. S. M., Wacker, L.,
869 Adolphi, F., Büntgen, U., Capano, M., Fahrni, S. M., Fogtmann-Schulz, A., Friedrich, R., Köhler, P.,
870 Kudsk, S., Miyake, F., Olsen, J., Reinig, F., Sakamoto, M., Sookdeo, A., and Talamo, S.: The
871 INTCAL20 Northern Hemisphere Radiocarbon Age Calibration Curve (0–55 cal kBP),
872 *Radiocarbon*, 62, 725–757, <https://doi.org/10.1017/RDC.2020.41>, 2020.
- 873 Reinig, F., Wacker, L., Jöris, O., Oppenheimer, C., Guidobaldi, G., Nievergelt, D., Adolphi, F.,
874 Cherubini, P., Engels, S., Esper, J., Land, A., Lane, C., Pfanz, H., Remmele, S., Sigl, M., Sookdeo, A.,
875 and Büntgen, U.: Precise date for the Laacher See eruption synchronizes the Younger Dryas,
876 *Nature*, 595, 66–69, <https://doi.org/10.1038/s41586-021-03608-x>, 2021.
- 877 Saarnisto, M.: Long varve series in Finland, *Boreas*, 14, 133–137,
878 <https://doi.org/10.1111/j.1502-3885.1985.tb00905.x>, 1985.
- 879 Saarnisto, M.: Annually laminated lake sediments, in: *Handbook of Holocene palaeoecology and*
880 *palaeohydrology*, edited by: Berglund, B. E., John Wiley and Sons Ltd, Chichester, 343–370, 1986.
- 881 Scharf, B.: *Limnologische Beschreibung, Nutzung und Unterhaltung von Eifelmaaren*,
882 *Ministerium für Umwelt und Gesundheit Rheinland-Pfalz, Mainz*, 1987.
- 883 Scharf, B. W. and Oehms, M.: Physical and chemical characteristics, in: *Limnology of Eifel maar*
884 *lakes. Ergebnisse der Limnologie*, vol. 38, edited by: Scharf, B. W. and Björk, S., E. Schweizerbart,
885 Stuttgart, 63–83, 1992.



- 886 Schmincke, H.-U.: The Quaternary Volcanic Fields of the East and West Eifel (Germany), in:
887 Mantle Plumes: A Multidisciplinary Approach, edited by: Ritter, J. R. R. and Christensen, U. R.,
888 Springer, Berlin, Heidelberg, 241–322, https://doi.org/10.1007/978-3-540-68046-8_8, 2007.
- 889 Schmincke, H.-U.: Vulkane der Eifel, 2nd ed., Springer, Berlin, Heidelberg, 2014.
- 890 Schnurrenberger, D., Russell, J., and Kelts, K.: Classification of lacustrine sediments based on
891 sedimentary components, *J. Paleolimnol.*, 29, 141–154,
892 <https://doi.org/10.1023/A:1023270324800>, 2003.
- 893 Shanahan, T. M., Beck, J. W., Overpeck, J. T., McKay, N. P., Pigati, J. S., Peck, J. A., Scholz, C. A., Heil,
894 C. W., and King, J.: Late Quaternary sedimentological and climate changes at Lake Bosumtwi
895 Ghana: New constraints from laminae analysis and radiocarbon age modeling, *Palaeogeogr.*
896 *Palaeocl.*, 361–362, 49–60, <https://doi.org/10.1016/j.palaeo.2012.08.001>, 2012.
- 897 Sirocko, F., Dietrich, S., Veres, D., Grootes, P. M., Schaber-Mohr, K., Seelos, K., Nadeau, M.-J.,
898 Kromer, B., Rothacker, L., Röhner, M., Krbetschek, M., Appleby, P., Hambach, U., Rolf, C., Sudo, M.,
899 and Grim, S.: Multi-proxy dating of Holocene maar lakes and Pleistocene dry maar sediments in
900 the Eifel, Germany, *Quaternary Sci. Rev.*, 62, 56–76,
901 <https://doi.org/10.1016/j.quascirev.2012.09.011>, 2013.
- 902 Stuiver, M., Reimer, P. J., Bard, E., Beck, J. W., Burr, G. S., Hughen, K. A., Kromer, B., McCormac, G.,
903 Van Der Plicht, J., and Spurk, M.: INTCAL98 Radiocarbon Age Calibration, 24,000–0 cal BP,
904 *Radiocarbon*, 40, 1041–1083, <https://doi.org/10.1017/S0033822200019123>, 1998.
- 905 Telford, R., Heegaard, E., and Birks, H.: All age–depth models are wrong: but how badly?,
906 *Quaternary Sci. Rev.*, 23, 1–5, <https://doi.org/10.1016/j.quascirev.2003.11.003>, 2004.
- 907 Trachsel, M. and Telford, R. J.: All age–depth models are wrong, but are getting better, Holocene,
908 27, 860–869, <https://doi.org/10.1177/0959683616675939>, 2017.
- 909 Vandergoes, M. J., Howarth, J. D., Dunbar, G. B., Turnbull, J. C., Roop, H. A., Levy, R. H., Li, X., Prior,
910 C., Norris, M., Keller, L. D., Baisden, W. T., Ditchburn, R., Fitzsimons, S. J., and Bronk Ramsey, C.:
911 Integrating chronological uncertainties for annually laminated lake sediments using layer
912 counting, independent chronologies and Bayesian age modelling (Lake Ohau, South Island, New
913 Zealand), *Quaternary Sci. Rev.*, 188, 104–120, <https://doi.org/10.1016/j.quascirev.2018.03.015>,
914 2018.
- 915 Zolitschka, B.: Spätquartäre Sedimentationsgeschichte des Meerfelder Maares (Westeifel).
916 Mikrostratigraphie jahreszeitlich geschichteter Seesedimente, *E&G Quaternary Sci. J.*, 38, 87–93,
917 <https://doi.org/10.3285/eg.38.1.08>, 1988.
- 918 Zolitschka, B.: Jahreszeitlich geschichtete Seesedimente aus dem Holzmaar und dem Meerfelder
919 Maar, *Z. Dtsch. Ges. Geowiss.*, 25–33, <https://doi.org/10.1127/zdgg/140/1989/25>, 1989.
- 920 Zolitschka, B.: Jahreszeitlich geschichtete Seesedimente ausgewählter Eifelmaare -
921 paläolimnologische Untersuchung als Beitrag zur spät- und postglazialen Klima- und
922 Besiedlungsgeschichte, Ph.D. thesis, Universität Trier, Documenta naturae, 60, 226, 1990.
- 923 Zolitschka, B.: Absolute dating of late Quaternary Lacustrine sediments by high resolution varve
924 chronology, 214, 59–61, <https://doi.org/10.1007/BF00050932>, 1991.
- 925 Zolitschka, B.: Climatic change evidence and lacustrine varves from maar lakes, Germany, *Clim.*
926 *Dynam.*, 6, 229–232, <https://doi.org/10.1007/BF00193535>, 1992.



- 927 Zolitschka, B.: A 14,000 year sediment yield record from western Germany based on annually
928 laminated lake sediments, *Geomorphology*, 22, 1–17, [https://doi.org/10.1016/S0169-](https://doi.org/10.1016/S0169-555X(97)00051-2)
929 [555X\(97\)00051-2](https://doi.org/10.1016/S0169-555X(97)00051-2), 1998a.
- 930 Zolitschka, B.: Paläoklimatische Bedeutung laminiertes Sedimente: Holzmaar (Eifel,
931 Deutschland), Lake C2 (Northwest-Territorien, Kanada) und Lago Grande di Monticchio
932 (Basilicata, Italien), *Habil. thesis, Universität Potsdam, Relief Boden Paläoklima*, 13, 176, 1998b.
- 933 Zolitschka, B., Haverkamp, B., and Negendank, J. F. W.: Younger Dryas Oscillation — Varve Dated
934 Microstratigraphic, Palynological and Palaeomagnetic Records from Lake Holzmaar, Germany,
935 in: *The Last Deglaciation: Absolute and Radiocarbon Chronologies*, edited by: Bard, E. and
936 Broecker, W. S., Springer Berlin Heidelberg, Berlin, Heidelberg, 81–101,
937 https://doi.org/10.1007/978-3-642-76059-4_6, 1992.
- 938 Zolitschka, B., Brauer, A., Negendank, J. F. W., Stockhausen, H., and Lang, A.: Annually dated late
939 Weichselian continental paleoclimate record from the Eifel, Germany, *Geology*, 28, 783–786,
940 [https://doi.org/10.1130/0091-7613\(2000\)28<783:ADLWCP>2.0.CO;2](https://doi.org/10.1130/0091-7613(2000)28<783:ADLWCP>2.0.CO;2), 2000.
- 941 Zolitschka, B., Francus, P., Ojala, A. E. K., and Schimmelmann, A.: Varves in lake sediments – a
942 review, *Quaternary Sci. Rev.*, 117, 1–41, <https://doi.org/10.1016/j.quascirev.2015.03.019>, 2015.
- 943